

Parity violation in proton-proton scattering at 45 MeV

R. Balzer, R. Henneck,* Ch. Jacquemart,† J. Lang, F. Nessi-Tedaldi, T. Roser, and M. Simonius
Institut für Mittelenergiephysik, Eidgenössische Technische Hochschule, 8093 Zürich, Switzerland

W. Haerberli

University of Wisconsin, Madison, Wisconsin 53706

S. Jaccard

Schweizerisches Institut für Nuklearforschung, 5234 Villigen, Switzerland

W. Reichart

Physikinstitut der Universität Zürich, 8001 Zürich, Switzerland

Ch. Weddigen

*Kernforschungszentrum Karlsruhe, Institut für Kernphysik und Institut für Experimentelle Kernphysik der Universität Karlsruhe,
 7500 Karlsruhe, Federal Republic of Germany*

(Received 18 June 1984)

Parity nonconservation in the pp interaction was studied by elastic scattering of 44.8 MeV longitudinally polarized protons. The scattering chamber consisted of a 100 bar H₂ gas target, surrounded by a cylindrical ionization chamber in an axially symmetric arrangement, and a Faraday cup. The relative cross sections, σ^+ and σ^- , for positive and negative helicity of the incident beam, were measured by integrating the current from the Faraday cup and from the ionization chamber during 20 ms intervals, and digitizing the charges. The parity nonconserving longitudinal analyzing power $A_z = (\sigma^+ - \sigma^-) / (\sigma^+ + \sigma^-)$ was deduced from 1.4×10^6 individual measurements of $p_z A_z$, where $p_z \simeq 0.83$ is the beam polarization. The emphasis is on quantitative treatments of instrumental effects, the most important of which is caused by the nonuniform distribution of residual transverse polarization components in the beam. The final result for the helicity dependence of the total nuclear pp cross section at a laboratory energy of 44.8 MeV is $A_z^{\text{tot}} = -(2.31 \pm 0.89) \times 10^{-7}$. The uncertainty includes the statistical error as well as the systematic uncertainties from transverse polarization, modulation of intensity, position, emittance, and energy of the beam associated with helicity reversal, double scattering, asymmetry from β decay, and electronic cross talk. The result is compared to theoretical predictions and to related experiments.

I. INTRODUCTION

It is well known that the strong nuclear interaction conserves parity to a high degree of accuracy. However, a small parity-violating component is expected from hadronic weak interactions, i.e., from a contribution to the nucleon-nucleon (NN) force by weak currents. Indeed, a number of experiments have clearly demonstrated parity violation in hadronic processes. In nuclear reactions, evidence for parity violation is provided by measurements of the circular polarization P_γ of γ rays from unpolarized radioactive sources, measurements of the asymmetry A_γ of γ rays from polarized nuclei, and the detection of parity-forbidden α decays (see Refs. 1–3 for reviews of these experiments). Even though the wrong-parity admixture in nuclear wave functions is very small (10^{-6} or so), the observed effects are enhanced in special cases where the parity-allowed transition is strongly hindered by other factors (e.g., isospin conservation). The most extreme enhancement of parity-violating effects relative to parity-allowed decays occurs in the decay of polarized metastable ^{180}Hf (Ref. 4), for which the observed γ -ray asym-

metry is $A_\gamma = -0.017 \pm 0.002$.

In recent years, the emphasis in experiments on parity violation in nuclear reactions has shifted from the mere illustration that an effect exists, to the much more ambitious task of elucidating the nature of the parity-violating components of the nucleon-nucleon interaction. Parity violation is, in fact, the only means to study strangeness-conserving purely hadronic weak processes. Theoretically, the problem is usually approached by describing the observed effects by the different isospin components of a weak (parity-violating) NN potential, and by relating these potentials to weak meson-nucleon coupling constants (π , ρ , ω , etc., exchange). This involves, even for the two-nucleon system, the understanding of the strong NN interaction at short distances, a problem of long standing interest by itself. Eventually, one hopes to compare the coupling constants so determined with predictions from weak interaction theories. This requires the evaluation of matrix elements of the weak Hamiltonian in the presence of strong interactions, a problem which is currently addressed by quantum chromodynamics (QCD). The comparison of these calculations with experiments is thus of

interest for weak and strong interaction physics.³

Parity experiments which show large, easily measured effects (such as A_γ in the decay of ^{180}Hf) are usually not amenable to interpretation in terms of a weak NN potential, because almost invariably the large suppression of the parity-allowed transition is associated with extremely complicated nuclear wave functions. Thus the emphasis centers now on experiments with selected light nuclei, for which the wave functions are thought to be accessible by means of modern nuclear structure calculations, and to the NN system itself. For all its attractiveness, the study of the NN system has the disadvantage that the expected effects are only of the order 10^{-7} and thus extremely difficult to observe.

For the n-p system, the experiments so far are limited to observations on γ rays from thermal n-p capture. A long-standing problem has been resolved recently. The old intriguing Leningrad measurements⁵ of the circular polarization of the outgoing gammas,

$$P_\gamma = (-1.30 \pm 0.45) \times 10^{-6},$$

has been recalled recently; a preliminary result of

$$P_\gamma = (1.8 \pm 1.8) \times 10^{-7}$$

is now obtained.⁶ At Grenoble, polarized cold neutrons were captured by unpolarized protons to measure the asymmetry

$$A_\gamma = (0.6 \pm 2.1) \times 10^{-7}$$

(Ref. 7). Current theories predict values well below 10^{-7} for both quantities.

For p-p scattering, parity violation has been studied through measurements of the helicity dependence of the elastic scattering cross section, i.e., the longitudinal analyzing power A_z as proposed by Simonius.⁸ This quantity is defined as

$$A_z = (\sigma^+ - \sigma^-) / (\sigma^+ + \sigma^-) \quad (1.1)$$

where σ^\pm is the total nuclear cross section for a longitudinally polarized incident proton beam with 100% polarization parallel (positive helicity) or antiparallel to the momentum vector.

The present paper reports on a series of experiments over several years, using protons with a mean energy of 44.8 MeV. The choice of bombarding energy is based on the fact that at low energies, A_z is known to reach a maximum near 50 MeV (Refs. 9 and 10). This statement is independent of any weak-interaction physics (which determines a multiplicative scale factor) and depends only on the known energy dependence of the strong 1S_0 and 3P_0 phase shifts. The first measurement of A_z was carried out at 15 MeV by a group at Los Alamos. They reported

$$A_z = (1 \pm 4) \times 10^{-7}$$

in a Letter¹¹ in 1974. Later work by the same group was reported only in conference proceedings,¹² the most recent result being

$$A_z = (-1.7 \pm 0.8) \times 10^{-7}.$$

In 1980, we published¹³ a value

$$A_z = (-3.2 \pm 1.1) \times 10^{-7}$$

for a proton energy of 45 MeV, while a group at Berkeley¹⁴ reported a preliminary result of

$$A_z = (-1.3 \pm 2.3) \times 10^{-7}$$

at 46 MeV. The present paper not only contains additional measurements, but presents a detailed treatment of instrumental effects and sources of error.

The principle of the experiment is described in Sec. II, while Sec. III contains details of the apparatus. A large part of the paper deals with the challenging problems that had to be solved to reduce the many systematic errors in A_z to the order of 10^{-8} (Sec. IV). Section V summarizes the procedures and results of the parity measurements, including error estimates from systematic effects. Section VI relates the results obtained so far to other measurements and to the theory of hadronic weak processes.

II. PRINCIPLE OF EXPERIMENT

The scattering cross section is proportional to N_s/N_p , where N_s is the number of protons scattered into the detector for N_p protons incident on the target. For our purposes, relative measurements of σ^+ and σ^- for positive and negative helicity are sufficient since common factors cancel in Eq. (1.1).

The basic arrangement is shown in Fig. 1. A gaseous H_2 target T is surrounded by a cylindrical ionization chamber IC. Integration of the current I_s in the ionization chamber gives a measure of the number N_s of scattered particles. Counting individual scattered protons is prohibitive since a few times 10^{14} protons have to be detected to reach the desired statistical accuracy in A_z . The number of incident protons N_p is measured by integrating the beam current I_p reaching the Faraday cup FC.

The use of a cylindrical detector surrounding the target has the advantage of a large solid angle (improved statistical error). In addition, the axial symmetry of the arrangement is essential to reduce systematic errors, such as the effects caused by possible small motion of the beam when the helicity is reversed. The fact that in our experiment the scattered particles are integrated over a wide range of angles involves no loss of information, since A_z is essentially independent of scattering angle,¹⁰ as long as one avoids very forward angles where Coulomb scattering dominates (see Fig. 3 and Sec. VI).

The polarized beam ($p \approx 0.83$) is provided by the injector cyclotron at Schweizerisches Institut für Nuklearforschung (SIN) equipped with an atomic-beam polarized-ion source (see, e.g., Ref. 15). Prior to ionization, the polarized neutral atomic beam, which is polarized in electron spin, is exposed to rf transitions between hyperfine states in order to obtain different proton polarizations. Alternately energizing so-called strong-field transitions (s) and weak-field transitions (w) allows rapid reversal of the proton polarization.

At the exit of the cyclotron, the transversely polarized beam is transformed into a longitudinally polarized beam (Fig. 1). The vertical beam polarization is precessed into

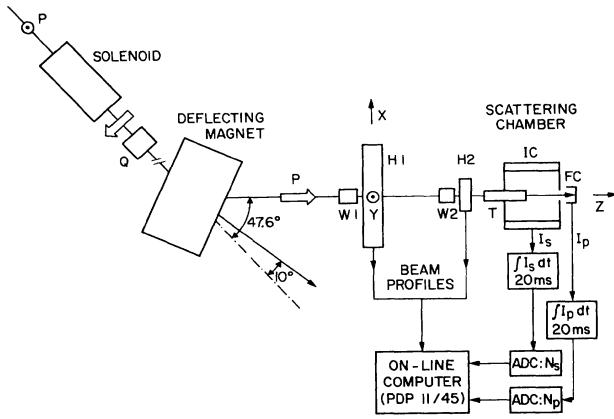


FIG. 1. Beam line and experimental setup to measure the longitudinal analyzing power A_z of elastic pp scattering at 45 MeV. The beam polarization P is shown for weak field transition w and Sol + : At the exit of the cyclotron P is oriented upwards (positive- y direction). The spin is precessed by the solenoid into the horizontal plane, and rotated into the positive z direction by the deflection magnet. The protons then pass through the pressurized H_2 target T and are stopped in the Faraday cup FC. The scattered protons are detected in the cylindrical ionization chamber IC. The beam scanners $H1$ and $H2$ measure the intensity and polarization profiles. The laminated quadrupole Q and two double-steering magnets $W1$ and $W2$ are used to measure sensitivities of the scattering chamber to spurious beam modulations. Beam scanners and the scattering chamber are moved to the 10° position to study the influence of horizontal polarization components.

the horizontal plane by passing the beam through the bore of a solenoid (effective length 0.91 m, mean field 0.65 T). Longitudinal polarization is obtained by deflecting the beam through a suitable angle (47.6°). Depending on the sense of the solenoid current, a spin-up polarization at the cyclotron exit is transformed into either a positive or negative helicity at the scattering chamber.

The helicity is reversed periodically (nominally every 30 ms) by switching rf transitions at the ion source. Charges proportional to N_p and N_s are determined by integrating I_s and I_p over 20.0 ms. After each such 20 ms measurement, a roughly 10 ms dead time is introduced, during which the digitized values of N_p and N_s are transmitted to the computer, the integrators are reset, the helicity is reversed, and beam scanners move through the beam to determine profiles of beam intensity and transverse polarizations.

To suppress periodic noise, the regular reversal between positive and negative helicity is maintained only for four cycles, after which the phase is reversed (see Sec. IV H). After eight cycles, the initial sign for the next group of eight cycles is chosen by a pseudorandom number generator.

In order to make explicit the conditions under which the experiments were performed, the following definitions are used:

(i) Superscripts w and s will be used to indicate whether the weak-field or the strong-field transition was energized.

(ii) From the physics of the rf transitions¹⁵ it is known that s corresponds to proton polarization along the magnetic field in the ionizer of the polarized ion source, while w corresponds to opposite polarization.

(iii) For all measurements reported here, the magnetic field in the ionizer was oriented downwards. Thus, w corresponds to beam polarization prior to the precession solenoid oriented upwards, while s corresponds to polarization oriented downwards. The sign of polarization was checked by p - ^{12}C elastic scattering at 45° . It is consistent with the sign of the analyzing power reported in Ref. 16.

(iv) The magnetic field in the precession solenoid is called positive (Sol + or superscript +) if a polarization oriented upward at the exit of the cyclotron is precessed into a beam of positive helicity p_z . For our arrangement (Fig. 1) Sol + corresponds to a solenoid field direction opposite to the momentum of the protons.

(v) For Sol +, switching from w to s corresponds to switching from positive to negative helicity p_z . Reversing the solenoid current reverses p_z , i.e., $p_z^{w,+}$, $p_z^{s,-} > 0$; $p_x^{w,-}$, $p_x^{s,+} < 0$.

We define as the primary measured quantity the ratio

$$R^\pm = \frac{(N_s/N_p)^w - (N_s/N_p)^s}{(N_s/N_p)^w + (N_s/N_p)^s}, \quad (2.1)$$

where R^+ and R^- refer to measurements made with Sol + and Sol-, respectively. In practice, the observed ratios R contain, besides the parity-violating effect R_z associated with the helicity reversal of the beam, also a contribution R_I from unwanted instrumental effects:

$$R^\pm = R_z^\pm + R_I^\pm. \quad (2.2)$$

In particular, R_I contains contributions from small transverse polarization components in the beam. Other contributions to R_I can arise if switching between w and s causes changes in the beam characteristics (e.g., beam intensity modulation).

If the incident beam has only a longitudinal polarization p_z (i.e., $p_x = p_y = 0$), the total nuclear cross section is

$$\sigma_z = \sigma_0(1 + p_z A_z), \quad (2.3)$$

where σ_0 is the cross section for an unpolarized beam. If (N_s/N_p) in Eq. (2.1) is proportional to σ_z , R_z^\pm can be written as

$$R_z^\pm = \frac{p_z^\pm A_z}{1 + \delta p_z^\pm A_z} \simeq p_z^\pm A_z, \quad (2.4)$$

where p_z^\pm and δp_z^\pm are defined as

$$p_z^\pm = \frac{1}{2}(p_z^{w,\pm} - p_z^{s,\pm}), \quad (2.5)$$

$$\delta p_z^\pm = \frac{1}{2}(p_z^{w,\pm} + p_z^{s,\pm}). \quad (2.6)$$

To a good approximation

$$p_z^+ = -p_z^- = p_z, \quad (2.7)$$

because the polarized ion source is stable over long periods of time. We rewrite Eq. (2.2) in terms of the effective beam polarization p_z as

$$R^\pm = \pm p_z A_z + R_I^\pm \quad (2.8)$$

or

$$A_z = \pm(R^\pm - R_I^\pm)/p_z = \pm R_z^\pm/p_z. \quad (2.9)$$

To obtain the final result for A_z we average measurements obtained with positive and negative solenoid fields,

$$A_z = [(R^+ - R^-) - (R_I^+ - R_I^-)]/2p_z = [R_z^+ - R_z^-]/2p_z. \quad (2.10)$$

We note that instrumental effects R_I which can be assumed invariant under reversal of the solenoid field direction (e.g., effects caused by beam intensity variation between states w and s), cancel in the final result.

III. APPARATUS

A. Scattering chamber

The scattering chamber is shown to scale on the right-hand side of Fig. 2. The H_2 target T consists of a 60 mm diameter cylinder of 1 mm wall thickness. The entrance and exit foils have a diameter of 24 and 60 mm, and a thickness of 0.17 and 1 mm, respectively. The target cell, including its windows, is made of high tensile strength (5.5×10^8 N/m²) aluminum alloy.¹⁷

The nominal target pressure for parity measurements was 100 bar. Care was exercised to achieve a pressure target of accurate cylindrical symmetry. The wall thickness was measured with an ultrasonic probe and was found to be uniform to 10 μ m over the entire surface. An entrance collimator with two tungsten apertures shields the ioniza-

tion chamber (IC) from protons scattered in the entrance window. Shields around the exit window serve a similar purpose. These apertures and shields also stop electrons and positrons which are produced by activation of the entrance and exit windows. The relatively large diameters of target cell and Faraday cup (FC) are desirable because of multiple scattering of the beam in the target. The diameter of the Faraday cup is such that the flux of protons at the edge of the cup is 10^{-4} compared to the flux on the chamber axis.

For the ionization chamber, a large diameter is of advantage because it reduces the effects caused by small displacements of the beam from the axis. The ionization chamber consists of a cylindrical ion collector of 40 cm diameter and an inner electrode of 36 cm diameter at +10 kV, filled with hydrogen at atmospheric pressure. The length (18.3 cm) of the ionization volume is defined by guard rings. The inner electrode consists of a thin Al foil F , stretched over 60 taut stainless steel wires of 0.5 mm diameter. The spacing between the wires and the collector was measured to be homogeneous to within 0.15% over the entire circumference. The uniformity of this spacing determines the homogeneity of the ionization volume, i.e., the variation of the efficiency as a function of the azimuthal angle. A small inhomogeneity in the ionization chamber results from the joint of the ends of the Al foil along a line parallel to the chamber axis.

The proton beam is stopped by a tungsten beam stop in the Faraday cup. Secondary electrons are suppressed either by an electrostatic suppressor (-1 kV) or a transverse magnetic field (~ 1 mT). A stainless steel cylinder C shields the ionization chamber against electrons and positrons emitted from the beamstop. The pressure in the Faraday cup is below 10^{-5} mbar, so that the current due to ionization of residual gas is below 10^{-4} of the proton current.

A computer program was written to calculate various properties of the scattering chamber (angular acceptance, I_s/I_p , sensitivity to residual transverse polarization and to energy modulations). The number of ion pairs produced in the ionization chamber by a beam of infinitesimal transverse dimensions and arbitrary position was computed by numerical integration over the path in the target and the volume of the ionization chamber. Energy-loss and range data were taken from Ref. 18, while data on the pp cross section and analyzing power as a function of energy (38.2–49.5 MeV) were calculated from the phase shifts of Arndt *et al.*¹⁹

The calculated acceptance function of the ionization chamber as a function of scattering angle is shown in Fig. 3. Whereas the smallest angle is defined by geometry, the upper limit on angle is given by the fact that beyond 52° all scattered protons are stopped before they reach the ionization chamber. Since the protons ionize most heavily at the end of their range, the acceptance function is strongly peaked near the maximum angle.

The current I_s in the ionization chamber, relative to the incident current I_p , was calculated, assuming that 37 eV are required to form an ion pair in H_2 (Ref. 20). Multiple scattering and range straggling were neglected in the calculation. Taking into account the approximations in this

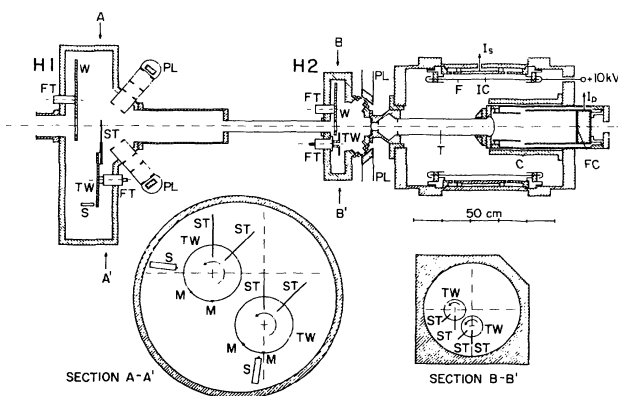


FIG. 2. Details of the beam scanners $H1$ and $H2$ and of the scattering chamber. The scanners contain two wheels TW . Two carbon strip targets ST are attached to each wheel to scan profiles of beam intensity and polarization in the vertical and horizontal directions. The wheels are driven by stepping motors through rotary feedthroughs FT . The rotation is monitored by magnetic sensors S and markers M , shown only for $H1$. When passing through the beam, the targets ST are viewed by two pairs of scintillation detectors coupled to the light pipes PL . Only the up-down detector pairs are shown. Auxiliary wheels W serve to introduce targets or apertures into the beam for test runs. The scattering chamber contains the target vessel T , the cylindrical ionization chamber IC with an aluminum foil F as inner electrode, and the Faraday cup FC with tungsten beamstop. The stainless steel cylinder C hinders β particles from activation in the FC to affect the current I_s .

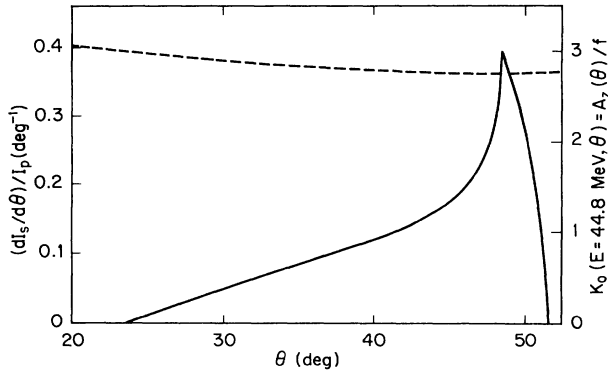


FIG. 3. Angular dependence of the longitudinal analyzing power $A_z(\theta)$ and acceptance function $(1/I_p)dI_s/d\theta$ of the detection system as a function of laboratory scattering angle. The scale for the acceptance function is shown on the left. The dashed line shows the angular dependence of the longitudinal analyzing power K_0 ($E=44.8$ MeV, θ) = $A_z(\theta)/f$ (scale on the right), as discussed in Sec. VI.

calculation, the predicted ratio $I_s/I_p=2.95$ is in reasonable agreement with the measured value of 2.05.

B. The polarized ion source

The ion source is an atomic-beam type of polarized ion source external to the cyclotron. Beam currents on target of 0.7–1.4 μA were achieved by use of a modern high-efficiency electron bombardment ionizer.²¹ Ionization of the polarized hydrogen atoms takes place in a magnetic field of 0.15 T, i.e., large enough to decouple electron and nuclear spin.

The hydrogen atomic beam emerging from the spin-separation magnet is polarized in electron spin only, i.e., it contains equal numbers of atoms in hyperfine state 1 (strong field quantum numbers $m_j = +\frac{1}{2}$, $m_I = +\frac{1}{2}$) and state 2 ($m_j = +\frac{1}{2}$, $m_I = -\frac{1}{2}$), where we use the notation of Ref. 15. Net nuclear polarization is obtained by exposing the atomic beam to rf transitions prior to ionization. The weak-field transition (adiabatic transitions between states 1 and 3) reverses m_j and m_I for atoms in state 1, leading to $p^w \simeq -1$ with respect to the magnetic field in the ionizer. The strong-field transition (2→4) reverses m_j and m_I for atoms in state 2 and thus leads to $p^s \simeq +1$. In our case, the two rf oscillators are energized alternately, thus switching the sign of proton polarization every 30 ms.

The beam polarizations p^w and p^s are measured with the beam scanners (precession solenoid turned off). Typically, the effective polarization $p_z \simeq 0.83$. The quantity $\delta p_z \simeq \delta p_z^+ \simeq -\delta p_z^-$ [Eq. (2.6)] depends sensitively on the tuning of the rf transitions. Under typical conditions, $|\delta p_z| \simeq 0.02$, but values as high as 0.04 occurred at times.

To ascertain that the beam polarization reaches its final value rapidly after polarization reversal, $p(t)$ was measured using a stationary thin graphite target instead of the moving carbon strip targets T in Fig. 2. The rise time of the polarization was found to be 0.2 ms, as expected from the spread in flight time of atoms between the rf transi-

tion unit and the ionizer. No other time structure is observed. Measurements exactly synchronous with the line frequency were also made, in order to ascertain that the beam polarization shows no time structure associated with line frequency, e.g., from stray fields affecting the weak-field transition unit.

C. Beam scanners and beam line

It is basic to the present experiment to determine if the properties of the proton beam (residual transverse polarization components, beam position, beam diameter, etc.) exhibit changes associated with the reversal of the helicity, since such changes give a contribution to R . The required information is provided by specially designed digital beam scanners, which are shown in proper relation to the scattering chamber in Fig. 2. These scanners are mounted as a rigid unit on the same cast-iron surface plate that carries the scattering chamber. This plate in turn is mounted on a subcarriage in such a way that the plate can be moved in all dimensions by remote control. The motion of the plate relative to the subcarriage is measured to ± 10 μm , to permit controlled motion, e.g., to align the chamber along the beam axis.

Two scanners, labeled $H1$ and $H2$, are 0.96 and 0.11 m from the target entrance, respectively. The scanning wheels TW, shown in Fig. 2, are driven by stepping motors. The time per revolution is 240.4 ± 0.3 ms. Protons which are scattered elastically from the graphite scanning strips ST are detected in scintillation detectors. The scattering angle is chosen to correspond to the maximum in the $p+^{12}\text{C}$ analyzing power of

$$A_C = 0.93 \pm 0.02 \quad (3.1)$$

at our bombarding energy of 50.7 ± 0.1 MeV. The value of the analyzing power was calculated from data in Ref. 16. The exact location (50.4°) of the analyzing power maximum was independently determined to $\pm 0.2^\circ$ in our own experiment. For each scanner, four scintillation detectors with an acceptance of $\pm 1.1^\circ$ were used to measure the spatial distributions $p_x(x)$, $p_x(y)$, $p_y(x)$, and $p_y(y)$ as discussed in Sec. IV A, as well as the corresponding intensity distributions. The phase angles of the four wheels are fixed and synchronized to the parity measurements such that one target passes through the beam during the 10 ms dead time which follows each 20 ms parity measurement. Magnetic sensors S , which respond to markers M on the wheels, provide a start signal prior to each target pass through the beam. These signals start (after an adjustable delay) an encoder which digitizes the position of the targets associated with each detected proton. The channel width of the digitizer is 58.4 μs which corresponds to a motion of 0.31 and 0.10 mm per channel, respectively, in scanners $H1$ and $H2$. The number of channels processed is 128, corresponding to a scan time of 7.48 ms. After a scan, the beginning of another 20 ms parity measurements is triggered.

The beam scanners are identical to those described in Ref. 22, except that the scan speed has been changed, and that two encoders in parallel are used to permit higher

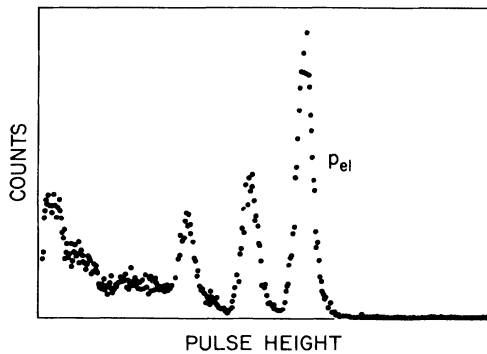


FIG. 4. Pulse height spectrum from one scintillation detector of the beam scanner *H2* (Fig. 2). The peak labeled p_{el} , which corresponds to proton elastic scattering from ^{12}C , is well separated from inelastic scattering to the 4.4 MeV excited state of ^{12}C . The third peak is an artifact of collimator design (penetration of thin aperture used in order to reduce slit edge scattering).

count rates. The rate per detector of elastically scattered protons when a target is in the center of the beam is about 50 kHz. To reduce gain shifts, each photomultiplier with its associated amplifier and single channel analyzer is equipped with a stabilization circuit. Figure 4 shows a typical pulse-height spectrum from a detector in the scanner *H2*. The elastically scattered protons are clearly separated from inelastic scattering to the first excited state of ^{12}C . An example of typical intensity and polarization profiles is shown in Fig. 5.

Prior to entering each beam scanner, the beam passes through magnets *W1* and *W2* which are indicated schematically in Fig. 1, but which are omitted in Fig. 2. Each of these so-called wobble magnets permits rapid modulation of the beam position for test purposes. Focus modulation for test purposes is provided by a quadrupole lens *Q*. These magnets are driven by programmable power supplies, and permit beam position modulation for alternate 20 ms parity measurements. The rise time of the magnetic fields is $\lesssim 1$ ms.

D. Current integrators

The currents I_p and I_s in the Faraday cup and ionization chamber, respectively, are integrated over a well-defined interval of 20.0 ms. The output voltages of the integrators are read at the beginning and end of each integration time in order to eliminate zero-drift errors. After the voltages are read and stored by a sample-and-hold amplifier, they are digitized by analog-to-digital converters (ADC's). Finally the digital data are transferred to the CAMAC system connected to a PDP 11/45 computer.

The resettable integrators were constructed using field-effect transistor (FET) operational amplifiers (selected Teledyne-Philbrick 142 502) and FET switches (Siliconix DG 200). The low bias current and the high gain bandwidth product help to keep nonlinearities of the integrators small (differential nonlinearity $\sim 10^{-4}$). The analog-to-digital conversion is carried out by commercial 16-bit

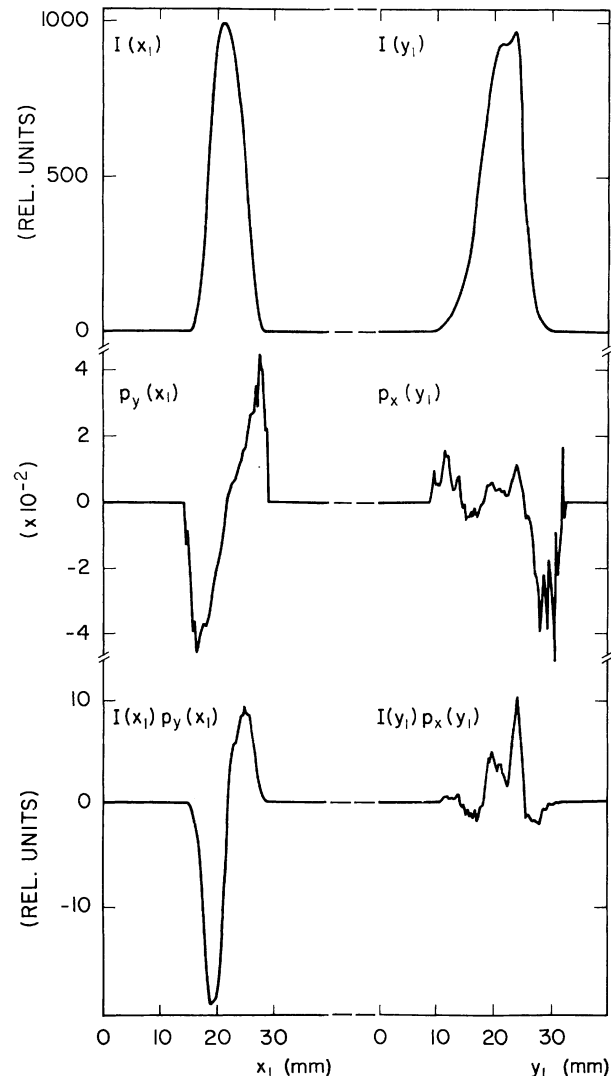


FIG. 5. Intensity and polarization profiles of the beam as measured by the first beam scanner in a 20 min run with $1 \mu\text{A}$ beam current.

ADC modules (Analog MP 8037).

Special precautions were taken in order to reduce errors from the pickup of interfering signals. All digital signals are insulated from the analog part by optocouplers or pulse transformers. In particular, the serial data transfer to the CAMAC system makes use of a fiber optics transmission line. Finally, low capacitance insulation transformers are used between the power supplies and the mains.

The resolution of the ADC's is much coarser than is required to detect effects of the order 10^{-7} . However, in view of the statistical accuracy of each 20 ms measurement, the additional error caused by the resolution of the digitizing process is small (see Sec. VB). In addition, the discrete boundaries of the digitizers are smeared out by adding white noise (of some 100 channels in width) to the reset voltage of the integrators, so that the initial voltage of the integrators varies randomly.

In the experiment, the beam current I_p , and correspondingly the ionization chamber current I_s , fluctuates. In addition, the beam current changes slightly ($\approx 10^{-4}$) when the beam polarization is switched from w to s . For these effects to cancel in the ratio N_s/N_p , the electronic system must possess a great degree of linearity. As a test of the entire system we measure the common-mode rejection with modulated current sources connected to both integrators. The spurious signal remaining in N_s/N_p is found to be roughly 10^{-4} of the amplitude of the modulations in N_s and N_p separately. In the actual parity measurements, more stringent tests are made periodically by modulating the intensity of the beam from the cyclotron.

For the first measurements (series 1), an earlier version of the system was used, which employed 14-bit ADC's. The common-mode rejection of the earlier system was an order of magnitude worse.

IV. SYSTEMATIC ERRORS

The study of possible sources of systematic errors is the most important aspect of the experiment described here. In fact, the majority of beam time is devoted to these problems. In particular, it is crucial to determine if reversal of the helicity by switching between w and s causes other changes in the beam, which could give a contribution to the measured value of R . Whenever possible our philosophy is not to rely on plausibility arguments about the behavior of the ion source and the cyclotron. Rather, the beam properties are sampled continuously during the parity runs in order to detect coherent modulations of the beam, i.e., modulations in step with the helicity reversal. The sensitivity of the scattering chamber to various beam modulations is measured in auxiliary experiments, by introducing artificial modulations of the intensity, position, diameter, and transverse polarization of the beam, combined with deliberate beam misalignments. This is done even in those cases where no modulation was discovered, in order to assign upper limits to the corresponding systematic errors.

We first explain the treatment of effects caused by the presence of residual transverse polarization components p_x and p_y in the longitudinally polarized beam (Sec. IV A). They cause the only significant corrections to the results of the parity measurements. We also consider coherent modulation in beam intensity (Sec. IV B), and coherent modulation in beam position and beam emittance (Sec. IV C). The possibility of coherent modulation in beam energy is considered (Sec. IV D).

Certain other effects could not be monitored during the parity runs but required auxiliary measurements. One such effect arises from double scattering of protons in the chamber, combined with a possible deviation of the scattering chamber from axial symmetry (Sec. IV E). Another effect (Sec. IV F) deals with a possible error caused by parity violation in β decay, since β emitters are produced in all parts of the chamber exposed to incident or scattered protons. The problems of electronic cross talk and insufficient averaging of possible (incoherent) line-frequency modulation in the beam are discussed (Secs. IV G and IV H). Finally, background effects were

measured with an empty target (Sec. IV H).

The various contributions to the corrections R_I for systematic errors [Eq. (2.2)] will be denoted by R_i , where the subscript refers to the effects mentioned above. In order to make explicit under what conditions corresponding sensitivities and modulations are obtained, we use the following notation:

(i) A "measurement" consists of a 20.0 ms integration period for the currents I_s and I_p .

(ii) A "cycle" of 30.045 ms (see Sec. IV H) includes additional 10 ms of beam scanning and dead time.

(iii) A "run" takes 20 min and consists of 40 320 cycles.

(iv) A "series" is the result of a block of cyclotron beam time. Series 1 (2) comprises 34 (35) parity runs. Each series consists of two subseries obtained with opposite solenoid excitations.

An overall summary of the systematic errors is presented with the parity results in Sec. V C.

A. Transverse polarization components

Ideally, the beam is polarized exactly along the z direction. However, there are present in the beam inevitable small transverse polarization components p_x and p_y which presumably change sign in step with the helicity and thus can cause erroneous signals. Transverse beam polarization, say p_y , causes a left-right asymmetry in p-p scattering as a result of the normal (parity-conserving) analyzing power A_y . The weighted mean of the p-p analyzing power for the angular range used in the present experiments is $A_y \approx 0.006$. As a consequence, the intensity scattered to the left is increased by a fraction $p_y A_y$, while the intensity on the right is decreased by the same amount. This shift of intensity from right to left is of no consequence provided the beam axis coincides with the chamber axis. However, if the beam is displaced from this axis by a small amount δx , there will be a false signal proportional to $(p_y \delta x) A_y$, because detector solid angle and proton energy at the detector will be different for left and right. Since the false signal is proportional to the first moment of p_y with respect to x displacement, an erroneous signal remains even for a perfectly centered beam and with mean polarization $\langle p_y \rangle$ equal to 0, if the polarization $p_y(x)$ varies, e.g., linearly, with x (see Fig. 5). It should be emphasized already at this point that the largest effects arise not from beam misalignment or a remaining mean transverse polarization, but from variation of the transverse polarization $p_y(x)$ and $p_x(y)$ across the beam.

We will denote the contribution to R_I , which arises from this type of effect, by R_T . To determine R_T , and to correct the measurements accordingly, requires two steps: (1) continuous measurement of the intensity distributions and transverse polarization distributions of the beam during the parity measurements, and (2) auxiliary experiments with a transversely polarized beam to measure the sensitivity of the chamber to transverse polarization as a function of beam position in the chamber. Our treatment is based on a paper²³ which presents a general mathematical treatment of the problem. This treatment shows that R_T can be expressed, to a good approximation, as [see Eq. (47), Ref. 23]

$$R_T = a_y^0 \langle p_y \rangle + a_y^{x_1} (\langle p_y \rangle \langle x_1 \rangle + \langle p_y \xi_1 \rangle) + a_y^{x_2} (\langle p_y \rangle \langle x_2 \rangle + \langle p_y \xi_2 \rangle) \\ + a_x^0 \langle p_x \rangle + a_x^{y_1} (\langle p_x \rangle \langle y_1 \rangle + \langle p_x \eta_1 \rangle) + a_x^{y_2} (\langle p_x \rangle \langle y_2 \rangle + \langle p_x \eta_2 \rangle), \quad (4.1)$$

where the coordinates x_1 , x_2 , etc., are beam coordinates measured in the two beam scanners as shown schematically in Fig. 6. The coordinates of the center of gravity of the beam are denoted by $\langle x_1 \rangle$, $\langle y_1 \rangle$, etc., while the quantities ξ and η are coordinates with respect to the center of gravity,

$$\xi_i = (x_i - \langle x_i \rangle), \\ \eta_i = (y_i - \langle y_i \rangle). \quad (4.2)$$

Thus the terms containing ξ and η describe intrinsic properties of the beam, which cannot be altered by adjusting the beam position in the chamber.

The origin of the coordinate system is assumed to be close to, but not necessarily coincident with, the optical alignment axis of the scattering chamber. The first term on each line of Eq. (4.1) arises from this misalignment of the scanner coordinate system with respect to the symmetry axis of the chamber. The remaining four terms correspond to beam displacements along $x_{1,2}$ and $y_{1,2}$. Each term consists of two contributions: the mean polarization $\langle p_y \rangle$ (or $\langle p_x \rangle$) multiplied with the beam misalignments $\langle x \rangle$ (or $\langle y \rangle$); and the intrinsic polarization moments of the beam $\langle p_y \xi \rangle$, $\langle p_x \eta \rangle$. The absence of moments of the form $\langle p_y y \rangle$ and $\langle p_x x \rangle$ is plausible since a left-right asymmetry combined with an up-down displacement has no effect provided the chamber is symmetric. The effect of these "harmless" moments, as well as the effects caused by higher-order moments, are for simplicity neglected in Eq. (4.1), but are taken into consideration in Ref. 23 and in the analysis below.

The six coefficients a_y and a_x in Eq. (4.1) describe the sensitivity of the scattering chamber to transverse polarization. The experimental determination of the sensitivities is based on measurements of R which are carried out exactly like parity measurements, but with deliberate large beam displacements and large transverse polarization. Large p_y is simply obtained by turning off the precession

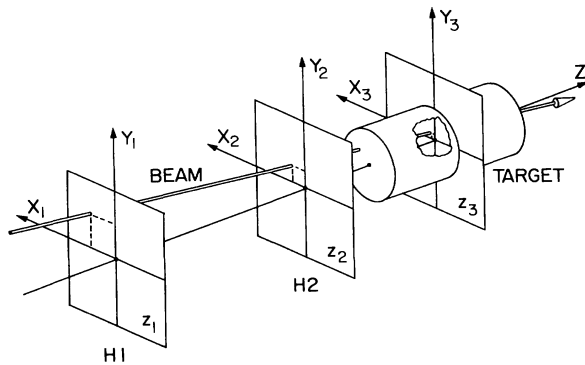


FIG. 6. Definition of coordinates in the planes z_1 and z_2 of the scanners $H1$ and $H2$, respectively. The significance of plane z_3 is explained in Sec. IV C.

solenoid (Fig. 1). To obtain large p_x is more complicated: the solenoid needs to be energized and the 47.6° deflection magnet turned off. Thus the entire scattering chamber has to be moved to a different beam port on the deflection magnet. Since a wall prevented the use of the 0° port, a 10° deflection was employed, resulting in a slightly reduced p_x compared to p_y .

A sample set of runs for a beam with vertical polarization $\langle p_y \rangle$ is shown in Table I. Note that the beam position is varied by moving the scattering chamber rather than by deflecting the beam. The uncertainties indicated on the second line are applicable to the remainder of the entries. One notes that R is large already for displacements of the order 2 mm, except when the displacement is primarily along the polarization direction.

For each series of parity measurements, the tests with a transversely polarized beam are repeated a number of times. The coefficients $a_{x,y}$ in Eq. (4.1) are determined by a least-squares fit to the data. In some cases as many as 20 runs were made with different beam coordinates relative to the chamber, including skew beams, to test for higher-order terms. It is found that Eq. (4.1) gives a satisfactory representation of all measurements, i.e., χ^2 per degree of freedom (7.7/9) is consistent with 1. The quality of agreement with Eq. (4.1) is illustrated by the last column of Table I.

In order to demonstrate how stable the sensitivities are under different experimental conditions, we show in Table II values obtained over a three-year period. The first double line represents averages over seven sets of a_y coefficients, determined during preliminary tests under different conditions: beam currents of 0.1, 0.3, and $0.8 \mu\text{A}$; variations of target pressure by 5%; measurements with and without circulating the H_2 target gas with a blower; measurements with and without a magnetic field of 1 mT applied over the chamber. The uncertainties in the first double line represent the variance of the coefficients under these differing conditions. The coefficients a_x^0 and a_y^0 for the preliminary tests varied substantially because the entire chamber was disassembled repeatedly during these tests without careful realignment, so that those particular coefficients are not comparable.

To correct the parity measurements, the coefficients are in each case determined under the actual conditions (target pressure, beam current, etc.) of the parity measurements. The coefficients on which the corrections for the parity series are based are listed in Table II. The last double line gives the result of a numerical calculation of the sensitivities mentioned in Sec. III A. The uncertainty in the calculation arises primarily from the need to use simplified energy-loss formulae. The calculations show that the sensitivity of the chamber to transverse polarization components arises essentially from differences in energy loss and from differences in solid angles.

Equation (4.1) is correct, including terms quadratic in the beam coordinates, if the apparatus has an axis of rota-

TABLE I. Example of measurements of R with beam polarization along y and different displacements $\langle x_1 \rangle$, $\langle y_1 \rangle$, etc., of the beam center. The last column shows the values of R after the correction R_T according to Eq. (4.1) has been applied. The errors given in the second line are characteristic for all entries in the same column. The last run is a typical parity run with $\langle p_y \rangle \simeq 0$.

Run No.	$\langle x_1 \rangle$ (mm)	$\langle x_2 \rangle$ (mm)	$\langle y_1 \rangle$ (mm)	$\langle y_2 \rangle$ (mm)	$\langle p_y \rangle$	R (10^{-7})	$R - R_T$ (10^{-7})
8122	-0.012 ± 0.003	0.029 ± 0.001	-0.031 $+0.003$	0.039 $+0.001$	0.818 ± 0.001	-0.135.8 ± 7.1	-9.1 \pm 7.2
8127	3.279	1.304	0.040	0.046	0.827	-555.2	-9.7 \pm 6.6
8135	-3.317	-1.071	0.047	0.067	0.834	246.2	7.4 \pm 6.9
8136	3.596	-1.087	0.084	0.074	0.834	472.0	9.6 \pm 7.0
8923	-0.096	-2.416	0.037	0.512	0.832	907.6	1.3 \pm 4.9
8924	-5.704	-0.038	-0.009	0.505	0.831	-247.7	-2.4 \pm 4.6
8931	0.260	-0.081	3.240	-0.553	0.832	-96.1	-1.2 \pm 4.6
8932	-0.022	-0.264	-0.006	-1.650	0.840	-30.0	2.4 \pm 4.6
8933	3.376	0.996	3.246	-0.598	0.822	-429.2	8.4 \pm 4.7
8298	0.012	0.003	0.329	0.011	-0.003	-8.3	-1.7 \pm 4.5
Mean							-0.8 \pm 1.7

tional symmetry. Symmetry requires $a_x^{y_1} = -a_y^{x_1}$ and $a_x^{y_2} = -a_y^{x_2}$. The conditions are met by the apparatus (Table II).

It is interesting to mention a problem observed in the preliminary tests with a different target cell of the same design: the large observed value of a_x^0 was traced to the fact that the bore in the target cell was displaced vertically by 50 μm , such that the wall was slightly thicker along the top of the target than the bottom. The present target cell is uniform in wall thickness to 10 μm .

Each parity run was corrected for residual transverse polarization, using the beam moments integrated over the run. Table III gives a summary of the various correction terms for series 2⁻. The uncertainties given arise from the statistical uncertainty in the determination of the beam moments. One notes that the correction is primarily caused by intrinsic polarization moments, and not from misalignment of either beam position or average polarization direction. For the other series the corrections were

similar, except that for series 2⁺ the beam had unusually large polarization moments $\langle p_y \xi_2 \rangle$ giving a mean contribution to R_T of $(-7.41 \pm 0.14) \times 10^{-7}$.

The corrections R_T for each run are several times larger than the desired final accuracy, but the corrections cancel to some extent when the results are averaged over all series. The net corrections for series 1 and 2 are

$$R_T = (0.32 \pm 0.08) \times 10^{-7}$$

and

$$R_T = (-1.73 \pm 0.09) \times 10^{-7},$$

respectively, where the uncertainties are statistical.

Systematic errors, which enter in these corrections, were studied in detail. The most important systematic uncertainties are the following:²⁴

(a) Uncertainties in the determination of the sensitivities add an additional error of $\pm 0.10 \times 10^{-7}$ to R_T .

TABLE II. Sensitivities of the apparatus to transverse polarization components, as defined by Eq. (4.1). The coefficients a_x^0 and a_y^0 are given in units of 10^{-7} , all others in units of 10^{-7} mm^{-1} . Changes of the values in the first column are associated with mechanical changes made on the system which affect the alignment of the beam scanners with respect to the scattering chamber.

Run time	a_x^0 a_y^0	$a_x^{y_1}$ $a_y^{x_1}$	$a_x^{y_2}$ $a_y^{x_2}$
Preliminary tests	3000	-44.5 \pm 1.3 47.7 \pm 1.6	587 \pm 10 -567 \pm 7
Series 1	-359.2 \pm 6.8 -0.1 \pm 5.4	-46.1 \pm 2.6 51.0 \pm 1.3	589 \pm 7 -576 \pm 4
Series 2	-383.4 \pm 4.9 -147.7 \pm 1.9	-40.6 \pm 1.0 41.0 \pm 0.6	562 \pm 10 -559 \pm 11
Calculated		-42 \pm 16 42 \pm 16	610 \pm 50 -610 \pm 50

TABLE III. Typical example of corrections for residual transverse polarization components. The contributions to the final correction R_T for a typical 20 min run and for series 2⁻ are tabulated. They were calculated from the measured polarization moments $\langle p_y \rangle$, $\langle p_y \rangle \langle x_1 \rangle$, etc., and the sensitivities a_x and a_y in Table II using Eq. (4.1).

Polarization moment	Run No. 8179		Average of series 2 ⁻	
	Measured moment ^a	Contribution to R_T (10^{-7})	Measured moment ^a	Contribution to R_T (10^{-7})
$\langle p_y \rangle$	0.98	-0.14 ± 0.06	1.10	0.16 ± 0.01
$\langle p_y \rangle \langle x_1 \rangle$	0.00	-0.79 ± 0.08	0.03	-0.43 ± 0.02
$\langle p_y \xi_1 \rangle$	-19.16		-10.45	
$\langle p_y \rangle \langle x_2 \rangle$	-0.30	0.63 ± 0.44	0.45	-0.93 ± 0.10
$\langle p_y \xi_2 \rangle$	-0.83		1.22	
$\langle p_x \rangle$	-3.47	1.33 ± 0.15	1.80	-0.69 ± 0.03
$\langle p_x \rangle \langle y_1 \rangle$	2.26	1.23 ± 0.09	1.02	1.05 ± 0.02
$\langle p_x \eta_1 \rangle$	-32.55		-26.78	
$\langle p_x \rangle \langle y_2 \rangle$	-1.03	-4.73 ± 0.26	1.01	-3.11 ± 0.06
$\langle p_x \eta_2 \rangle$	-7.39		-6.55	
Total		-2.47 ± 0.55		-3.96 ± 0.12

^aThe measured moments are given in units of 10^{-3} or 10^{-3} mm.

(b) There are additional systematic errors in the determination of the beam position and polarization moments. They arise from (i) background in the scintillation counters, (ii) a channel-dependent difference in the p-¹²C analyzing power for left and right detectors because of the systematic change in scattering angle with position of the target strip, (iii) systematic errors in beam properties because the scanning strips were assumed to undergo a parallel displacement while in fact they rotate about an axis, and (iv) finite resolution of the channels. The combined uncertainty of these effects is $\pm 0.10 \times 10^{-7}$.

(c) An uncertainty from the approximations in Eq. (4.1). The assumption that moments of the form $\langle p_y y \rangle$ and higher moments of the form $\langle p_y x^2 \rangle$, $\langle p_y y^2 \rangle$, and $\langle p_y x^3 \rangle$ can be neglected was tested experimentally. The total systematic uncertainty from these effects is $\pm 0.13 \times 10^{-7}$.

The quadratic sum of the above three systematic uncertainties in the correction R_T is 0.2×10^{-7} .

B. Intensity modulation

In first approximation the ratio N_s/N_p is independent of beam intensity. Thus, coherent beam intensity modulations should not affect A_z . However, residual effects arise, e.g., from (i) differential nonlinearity of the current integrators or analog-to-digital converters, (ii) dark currents either in the Faraday cup or in the ionization chamber, for instance, from activation of the chamber, and (iii) unmatched frequency response, for instance, a time delay between ion chamber and Faraday cup (finite collection time of ions).

We define the amplitude M_0 of the coherent beam intensity modulation as the mean modulation measured in the Faraday cup during a run,

$$M_0 = (N_p^w - N_p^s) / (N_p^w + N_p^s). \quad (4.3)$$

The measured values of M_0 are between -2×10^{-5} and -9×10^{-5} depending on adjustments of the ion source and the cyclotron. During a series of parity runs, M_0

varies typically by 1×10^{-5} .

The cause of the modulation is not entirely obvious, since in the atomic-beam apparatus the number of atoms that reach the electron-bombardment ionizer is unaffected by switching the rf transitions between w and s . A qualitative explanation is that the ionization probability of atoms in the different hyperfine states is different, because their average velocity, and thus the dwell time in the ionizer, is different on account of the interaction energy between the magnetic moments of the atoms and the 0.15 T magnetic field in the ionizer. It is readily seen from the Breit-Rabi diagram (e.g., Fig. 1 of Ref. 15) that the expected intensity modulation is much smaller when one alternates between w and s , than when either transition is turned off permanently. Indeed, it was found that M_0 increases by at least an order of magnitude when one rf transition unit is switched, the other permanently turned off.

The sensitivity of the scattering chamber to M_0 is described by a coefficient K_0 ,

$$R_0 = K_0 M_0, \quad (4.4)$$

where R_0 is the contribution to R_I [Eq. (2.2)] due to intensity modulation. To measure K_0 , artificial intensity modulations of different amplitudes M_0 were made and R was measured. The intensity was modulated in the following ways:

(i) One rf transition was turned off which resulted in $M_0 \simeq 1 \times 10^{-3}$, as mentioned above. The measured asymmetry R was corrected for effects of transverse polarization. Position modulation of the beam was negligible.

(ii) A pure intensity modulation of larger and reproducible amplitude ($M_0 = 5.0 \times 10^{-2}$) was produced by attenuating the neutral atomic beam with a fine wire mesh. The mesh was mounted on a rotating wheel whose motion was synchronized with the 30 ms measuring cycle.

(iii) A modulation M_0 of adjustable amplitude (2×10^{-3} to 7×10^{-2}) was produced by coherent modulation of the voltage applied to an electrostatic lens at the

exit of the ion source. This also introduces small modulations in beam position and beam diameter, but corresponding corrections to the asymmetry can readily be made (see Sec. IV C). For this and the preceding test, the rf transitions were turned off (unpolarized beam).

The above tests confirmed that R_0 varies linearly with M_0 . During the parity measurements, K_0 was measured periodically using methods (i) and (ii). In the early measurements (series 1), K_0 changed with beam current, since the differential linearity of the 14-bit ADC's was insufficient. Series 2, using rebuilt current integrators and new analog-to-digital converters, gave much more consistent values for K_0 . In addition, during the later runs, the intensity modulation during the parity runs was small, so that the corrections were almost negligible.

For series 1, the correction R_0 to each individual parity run was typically 1×10^{-7} . For comparison, the corrections were evaluated by using the value of K_0 determined nearest in time to the particular parity run, and by using the average value of K_0 for all measurements of the series. The difference in the final correction to the asymmetry R between the two methods was 0.03×10^{-7} .

Even though for series 1 the corrections R_0 were substantial, they largely cancel in the final result because these modulations, to the extent they are constant, have no effect after the results for Sol+ and Sol- are combined. The systematic uncertainties in the final results from intensity modulation are at most 0.2×10^{-7} for series 1 and 0.05×10^{-7} for series 2.

The above discussion tacitly assumed that in the parity measurements the intensity changes in a step-wise fashion upon switching the rf transitions. In order to study the response of the system to currents which change coherently during the 20 ms measuring time, the phase of the motor which inserts the grid into the atomic beam was altered such that an intensity change of 10% occurred during the 20 ms integration time. The measured values of R can be explained if one assumes a $5 \mu\text{s}$ time delay between Faraday cup and ionization chamber. Also, the dependence of beam current $I_p(t)$ after switching rf transitions was studied with a signal averager. No coherent slope in $I_p(t)$ during the 20 ms measuring time was detected. The error in the final result, calculated from a possible undetected coherent slope, is $< 10^{-10}$.

The $5 \mu\text{s}$ time delay is in qualitative agreement with the expected ion collection time in the ionization chamber. Since the time delay depends on the purity of the gas, the ionization chamber was continuously flushed with purified H_2 .

C. Position and emittance modulation

In this subsection we treat the effects caused by possible coherent changes in beam position or beam focus. The sensitivity of the scattering chamber to beam motion arises from the fact that the effective solid angle of the ionization chamber and the energy of the scattered particles in the ionization volume is a function of beam position in the target. For the parity measurements, the beam was sufficiently close to the symmetry axis of the chamber, and the measured upper limit of the coherent

position modulation was sufficiently small, that no significant corrections were required. Nevertheless, it is important to understand the response of the system to beam position modulation in order to analyze the possible effects caused by coherent emittance modulation, and to test the symmetry properties of the chamber.

The modulation in position and direction of the incident beam can be described in terms of the four beam coordinates $x_{1,2}$ and $y_{1,2}$ defined in Fig. 6. For each coordinate, we define a coherent position modulation, for example

$$M_{x_1} = \frac{1}{2} (\langle x_1 \rangle^w - \langle x_1 \rangle^s). \quad (4.5)$$

The effects of the modulation on R are, to first order, linear in M and linear in the displacement of the beam center from the axis of the apparatus, e.g.,

$$R_{x_1} = M_{x_1} (K_{x_1} + \langle x_1 \rangle K_{x_1}^{x_1} + \langle x_2 \rangle K_{x_1}^{x_2}). \quad (4.6)$$

Summed over all coordinates,

$$R_M = R_{x_1} + R_{x_2} + R_{y_1} + R_{y_2}. \quad (4.7)$$

The derivation²⁴ of Eq. (4.6) assumes that the scattering chamber is symmetric about the x - z and y - z planes, but allows for misalignment between scanners and scattering chamber (terms K_{x_1} , etc.).

Evaluation of R_M from the observed position modulations during the parity runs requires determination of the chamber sensitivities K . Since it can be shown²⁴ that $K_{x_1}^{x_2} = K_{x_2}^{x_1}$, and $K_{y_1}^{y_2} = K_{y_2}^{y_1}$, a total of ten coefficients needs to be determined. For this purpose we produce artificial position modulations with two pairs of (x,y) -steering magnets (wobble magnets $W1$ and $W2$, Fig. 1) and measure separately R_M for each modulation M_x , M_y , etc., for some 20 different sets of beam positions in the chambers. As an illustration, a typical 2 min run yields, e.g.,

$$R_M = (1384 \pm 16) \times 10^{-7}$$

for $\langle x_1 \rangle = 3 \text{ mm}$, $\langle x_2 \rangle = -1 \text{ mm}$, and an amplitude in magnet $W1$ of 0.27 mrad , which corresponds to $M_{x_1} = 0.06 \text{ mm}$, $M_{x_2} = 0.28 \text{ mm}$.

As an example, sensitivities determined from a fit to results of two sequences of test runs during series 2 are shown in Table IV. An additional 33 runs, which were interspersed with the parity runs, were also included in the fit. One notices that the conditions imposed by symmetry ($K_x^x = K_y^y$) are met. Again, as for the sensitivities to p_x and p_y , one notices the effects of misalignment between beam scanners and chamber ($K_x, K_y \neq 0$). As will be discussed in Sec. V A, the beam axis for the parity measurements was chosen to minimize the contribution from these terms.

Within the statistical accuracy of the measurements, there is no evidence for coherent position modulation during the parity measurements either in the individual runs, or in the average over an entire series. As an example, the results for series 2^+ and 2^- are shown in Table V which also gives the net correction to R after the results for Sol+ and Sol- are combined. The overall correction in

TABLE IV. Sensitivities K of the scattering chamber to position modulations, as defined in Eq. (4.6). The coefficients K_x and K_y are given in units of 10^{-7} mm^{-1} , all others in units of 10^{-7} mm^{-2} .

K_{x_1}	K_{x_2}	$K_{x_1}^{x_1}$	$K_{x_2}^{x_2}$	$K_{x_1}^{x_2} = K_{x_2}^{x_1}$
K_{y_1}	K_{y_2}	$K_{y_1}^{y_1}$	$K_{y_2}^{y_2}$	$K_{y_1}^{y_2} = K_{y_2}^{y_1}$
245 ± 26	-876 ± 17	-258 ± 15	-3520 ± 20	955 ± 10
-259 ± 27	1580 ± 16	-258 ± 12	-3460 ± 20	942 ± 6

Table V includes systematic errors in the sensitivities and in the determination of the modulations.

Originally, the chamber showed a pronounced lack of symmetry, in that the sensitivities to vertical motion (K_y) were much larger than could be explained by misalignment. The effect increased linearly with beam current. For a $1 \mu\text{A}$ beam, the effects became so large that to reach the desired accuracy in R_M of 1×10^{-8} would have required determination of the vertical beam modulation to $0.01 \mu\text{m}$, far less than the statistical error of the beam scanners. The cause of the problem was found to be a vertical temperature gradient of $0.3 \text{ K}/(\text{mm}\mu\text{A})$, which built up in 6 s after the beam was turned on. Addition of a blower, which circulates the target gas, solved the problem.

We now consider related effects which result from possible coherent modulation of the width or diameter of the beam, or “breathing” of the beam. The breathing amplitude is described by the coherent change in the second moments of the intensity distribution about the center of the beam. The magnitude of these effects cannot be obtained from the beam scanners, because the statistical accuracy in the determination of the second moments is insufficient. Furthermore, a complete analysis requires knowledge of correlated second moments between the two scanners. Our treatment of this problem makes use of two observations:

(i) The breathing amplitude in any plane z along the beam axis can be measured with high sensitivity in an auxiliary experiment, by inserting an aperture that intercepts part of the beam, and by measuring the modulation in the fraction of the beam passing through the aperture. In practice, apertures of 1 or 2 mm diameter were inserted immediately after scanner H_2 , and the entire scattering

chamber was moved along the z axis to the desired position.

(ii) It was found that there exists a plane $z = z_3$ (near the center of the gas target, see Fig. 6) for which modulation in angle about points in the plane has no effect on R . The existence of such a plane requires that $K_{x_1}^{x_2}$ in Eq. (4.6) equals the geometric mean of $K_{x_1}^{x_1}$ and $K_{x_2}^{x_2}$. This condition is satisfied by the coefficients in Table IV. Thus it is sufficient to measure beam breathing in a single plane z_3 . The amplitude of modulation is defined as

$$M_B = \frac{1}{2} (\langle \rho^2 \rangle^w - \langle \rho^2 \rangle^s), \quad (4.8)$$

where the radial coordinate ρ in the z_3 plane is measured with respect to the center of gravity of the beam,

$$\rho^2 = \xi^2 + \eta^2. \quad (4.9)$$

The effect, R_B , which beam breathing has on R is

$$R_B = K_B M_B, \quad (4.10)$$

where K_B can be calculated to first order from the known sensitivity to position modulation. The coefficients in Table IV yield

$$K_B = -(926 \pm 14) \times 10^{-7} \text{ mm}^{-2}.$$

During series 2 of the parity measurements the beam was tested periodically for breathing in the plane z_3 , 32 cm from z_2 . Neither the 1 mm nor the 2 mm aperture (intercepting 40% and 15% of the beam, respectively) showed measurable beam breathing:

$$M_B (1 \text{ mm aperture}) = (-40 \pm 32) \times 10^{-6} \text{ mm}^2, \quad (4.11)$$

$$M_B (2 \text{ mm aperture}) = (35 \pm 46) \times 10^{-6} \text{ mm}^2.$$

We assume $M_B < 50 \times 10^{-6} \text{ mm}^2$ and thus obtain an uncertainty in R from beam breathing of $\pm 0.05 \times 10^{-7}$ for series 2. For series 1, fewer test measurements were made, resulting in an uncertainty of $\pm 0.3 \times 10^{-7}$.

The above treatment rests on the assumption that the effects caused by modulations of beam position and beam breathing are closely related, i.e., the effects are basically geometric. To determine whether other effects (such as temperature gradients of the target gas within the beam) play a role, the validity of Eq. (4.10) and the value of K_B were tested in separate experiments by measuring R_B with artificial beam breathing produced with a small laminated

TABLE V. Coherent position modulation M of the beam. The mean values observed during the parity runs of series 2 are given in the top two lines. The last line gives the correction R_M calculated from Eqs. (4.2) and (4.4) using the sensitivities in Table IV. The errors of M are statistical, those of R_M include in addition the uncertainties of the sensitivities K .

Series	M_{x_1} (10^{-3} mm)	M_{y_1} (10^{-3} mm)	M_{x_2} (10^{-3} mm)	M_{y_2} (10^{-3} mm)	R_M (10^{-7})
2 ⁻	0.19 ± 0.31	0.34 ± 0.34	-0.14 ± 0.12	-0.17 ± 0.08	-0.20 ± 0.11
2 ⁺	-0.34 ± 0.31	-0.25 ± 0.43	0.10 ± 0.14	-0.19 ± 0.11	-0.01 ± 0.16
Net correction for series 2 (10^{-7})	-0.01	-0.08	-0.02	0.02	-0.09 ± 0.12

quadrupole magnet (Q in Fig. 1). The modulation M_B was measured with the beam scanner, and also with the aperture inserted in the beam, in order to test the validity of the aperture measurements. The results of all tests support the above treatment.

D. Energy modulations

It cannot be excluded *a priori* that the mean energy E of the protons changes when the polarized ion source is switched between w and s . Such a coherent energy modulation, $\Delta E = \frac{1}{2}(E^w - E^s)$, could give rise to an additional systematic error:

$$R_e = a_e(\Delta E/E). \quad (4.12)$$

The sensitivity to energy variation, a_e , is given by the variation of the pp cross section and the response function of the scattering chamber with energy. Using the same calculation that was applied to calculate the sensitivities to transverse polarization components, we obtain $a_e = -1.2 \pm 0.1$. Requiring $R_e < 10^{-8}$, therefore, leads to $(\Delta E/E) < 8.0 \times 10^{-9}$ or $\Delta E < 0.4$ eV.

In principle, one expects that the intrinsic energy modulation from an atomic-beam polarized ion source is negligible, since the energy difference for states w and s cannot be larger than $2\mu B$, where μ is the magnetic moment of the hydrogen atom and B the largest magnetic field (0.15 T) in the ion source, or $|\Delta E| < 2 \times 10^{-5}$ eV. However, it is conceivable that the protons emerging from the ion source are injected into the cyclotron with a small (coherent) phase space or position modulation which could lead to a small energy modulation of the beam after the accelerator.

While an energy modulation would be reflected in a position modulation, because the beam line contains dispersive elements, the beam scanners are insufficient to measure a modulation $\Delta E/E < 10^{-7}$.

If the field of the spin precession solenoid is reversed, the asymmetry due to energy variations, R_e , remains unchanged. It is, therefore, possible to deduce an upper limit for R_e from the average asymmetry R_{Sol} with positive and negative solenoid fields:

$$R_{\text{Sol}} = \frac{1}{2}(R_z^+ + R_z^-). \quad (4.13)$$

From series 1 and 2 we obtain

$$R_{\text{Sol}} = -(0.15 \pm 0.90) \times 10^{-7}$$

and

$$R_{\text{Sol}} = +(0.52 \pm 0.79) \times 10^{-7},$$

respectively (see Table VIII, Sec. V C). On the other hand, to obtain the parity violating part of the asymmetry we evaluate the expression $\frac{1}{2}(R_z^+ - R_z^-)$, where one has a cancellation of R_e , if the energy modulation has a sufficiently slow drift with time. The magnitude of the residual effect presumably depends on how often the sign of the solenoid is changed. Series 1 is made up of six subseries, three with a positive sign and three with a negative sign of the solenoid field, whereas series 2 contained only one subset with each field. We estimate that the residual error

due to energy modulation is $R_e < 0.2 \times 10^{-7}$ for series 1 and $R_e < 0.3 \times 10^{-7}$ for series 2.

Rapid (within a run) variations of the energy modulations are averaged out, but included as part of the statistical error in the final result. Finally, variations of R_e from run to run would increase the value of χ^2 for a series, which is not the case (see Sec. V B).

E. Double scattering

The scattered protons in p-p scattering have a polarization component transverse to their momentum which changes sign in step with the helicity reversal in the incoming beam even if the beam has no transverse polarization components. In this section we are concerned with effects which might arise if the scattered protons undergo a further scattering, e.g., in the wall of the target vessel, before reaching the detector. We must assume that this second scattering will produce a left-right asymmetry due to the nonvanishing regular analyzing power. Then, a false asymmetry R_D can arise if the protons which are scattered to the left (say) are not detected with the same efficiency as the ones scattered to the right (see Fig. 7).

If the incident proton beam is centered on the axis of the apparatus, double scattering produces no false asymmetry if either the target wall or the detector has exact axial symmetry. However, if the beam is not centered, the asymmetry disappears only if target and detector both have rotational symmetry.

In order to study this effect, and to obtain an estimate of its magnitude, we made a series of measurements where the asymmetries of the apparatus were deliberately enhanced. In one test a long strip of aluminum (T in Fig. 7) with a thickness of 0.2 mm and a width of 20 mm was placed on the surface of the target wall and in addition the ionization chamber was shielded by an aluminum rod

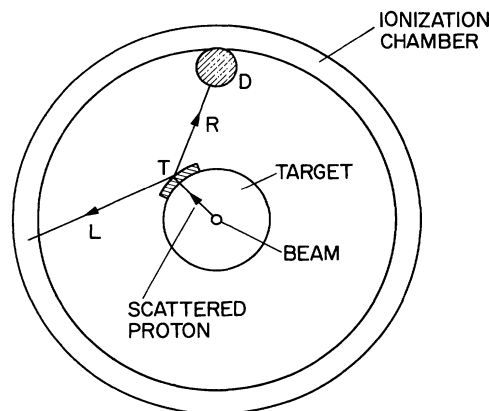


FIG. 7. Origin of a false asymmetry R_D due to double scattering. The helicity of the incident proton beam causes a transverse polarization of the scattered protons, which in turn results in a left-right asymmetry in the second scattering. The ionization chamber is sensitive to this asymmetry if it is not perfectly symmetric. For test purposes, artificial asymmetries were produced by inserting the Al strip T and the Al rod D into the scattering chamber.

D with a diameter of 20 mm at the position shown in Fig. 7. With this arrangement we measured an asymmetry

$$R = (48.7 \pm 7.0) \times 10^{-7}.$$

This value, corrected for the contribution R_T from transverse polarization components, yields an asymmetry:

$$R - R_T = (1.1 \pm 8.3) \times 10^{-7}.$$

It is essential that R_T be based on sensitivities measured for the modified arrangement, since use of the sensitivities for the symmetric arrangement leads to completely erroneous results.

We conclude from this measurement that the asymmetry due to double scattering is smaller than 10^{-6} for this special configuration. Since, to first order, this type of effect is proportional to the inhomogeneity of the target wall (which was enhanced by a factor 10) and to the asymmetry of the detector efficiency (enhancement factor ~ 10), the false asymmetry in the parity runs due to a similar configuration is $\leq 0.1 \times 10^{-7}$. Additional measurements where other artificial inhomogeneities in the equipment were introduced and with beams which were (simultaneously) deliberately misaligned, produced similar results.

We estimate an upper limit of 0.2×10^{-7} for possible systematic errors of this type. For series 1, the mounting of the inner electrode of the ionization chamber (joint in Al foil) introduced a larger asymmetry than the improved mounting used later. For series 1, the upper limit on R_D is therefore increased to 0.5×10^{-7} .

F. Asymmetry from beta decay

The incident longitudinally polarized protons produce short-lived polarized β -active nuclei in various parts of the scattering chamber. Because of the parity nonconserving asymmetry in β decay, the emitted electrons (or positrons) give a contribution to the current in the Faraday cup and the ionization chamber which depends on the helicity of the proton beam. Large effects are unlikely, because the fractional current which the β 's contribute to the Faraday cup and ionization chamber is small, and the spin relaxation time of the β emitters is expected to be very short compared to their lifetime, so that only a small fraction of the decays will show a helicity-dependent asymmetry. Moreover, for relaxation times much longer than the helicity reversal time, the effects would tend to cancel because in this case one averages over several helicity reversals.

The contribution R_β which β decays make to the measured ratio R can be calculated if one knows the effective activation cross section σ_β for the materials (W and Al) struck by protons, and the change in β -emission probability associated with the polarization reversal of the protons which produce the activity. The intensity of β 's emitted during a 20 ms integration time of the parity measurements can be expressed as

$$I^\pm(\vartheta) = I(1 \pm A_\beta \cos \vartheta), \quad (4.14)$$

where the superscript refers to the polarization of the incident proton beam, and ϑ is the β -emission angle with

respect to the time-averaged polarization direction of the β emitters. Note that A_β is defined operationally by the observed modulation under the special conditions of the parity experiment. It differs from the usual asymmetry parameter in β emission from completely polarized nuclei, since A_β contains, in addition, polarization transfer coefficients for the reactions producing the activity, relaxation of the activated nuclei, and averaging over the pattern of helicity reversals.

The required effective activation cross sections σ_β and asymmetries A_β were measured in a separate experiment, in which targets of Al and W were bombarded with polarized protons of different energies, and the number of β 's of energy > 0.5 MeV were counted in ΔE - E telescopes. Measurements of A_β were done with protons polarized parallel (A_β^{\parallel}) as well as perpendicular (A_β^{\perp}) to their momentum, since in the parity experiment the scattered protons have both components of polarization. The pattern of helicity reversal was identical to that used in the parity experiment, so that the measured A_β correspond exactly to the operational definition in Eq. (4.14).

The calculation of R_β from σ_β and A_β involves numerical integrations of the contributions which β decays make to the currents in the Faraday cup and the ionization chamber. The results can be expressed as a sum of terms of the form

$$R_\beta = K_\beta \sigma_\beta A_\beta, \quad (4.15)$$

where K_β depends on the geometry of the apparatus, as explained below.

The results of the calculations for the Faraday cup show that the largest contribution to R_β arises from β 's emitted by the 1 mm Al exit foil of the gas target. In this case, the calculated value of

$$K_\beta = 3.0 \times 10^{-4}/b$$

contains the Al target thickness, the solid angle which the Faraday cup extends from the Al foil, and the average value of $\cos \vartheta$. The test measurements yielded $\sigma_\beta = 0.02$ b for 50 MeV protons on a 1 mm Al target, and

$$A_\beta = (-1.0 \pm 1.4) \times 10^{-4}.$$

Thus R_β from this process is $< 2 \times 10^{-9}$. The corresponding limit for the W beam stop is $R_\beta < 3 \times 10^{-9}$. Contributions from other parts of the scattering chamber are much smaller.

The current measured in the ionization chamber contains roughly equal contributions from activation of the target wall and the inner walls of the scattering chamber by scattered protons. In this case the computation of K_β involves, besides purely geometric quantities, the ionization density of β 's in the ionization chamber and the pp scattering cross section. Also, since K_β includes the integration over $\cos \vartheta$, the pp spin rotation parameters enter. The pp data were calculated from the known pp phase shifts.¹⁹ The calculated values are

$$K_\beta^{\parallel} = 0.7 \times 10^{-4}/b$$

and

$$K_\beta^{\perp} = -0.3 \times 10^{-4}/b$$

where the superscript again refers to polarization components of the scattered protons parallel or perpendicular to their momentum. The effective activation cross section for proton energies 25, 40, and 50 MeV and Al targets of 1 and 20 mm thickness were all <0.03 b, and the values of A_β were all consistent with zero. If we assume $A_\beta < 2 \times 10^{-4}$ [the measured average values were

$$A_\beta^{\parallel} = (0.3 \pm 0.6) \times 10^{-4}$$

and

$$A_\beta^{\perp} = (1.1 \pm 0.6) \times 10^{-4},$$

we obtain $R < 10^{-9}$ for the ionization chamber.

The above results do not yet make use of the fact that a 1 mT transverse magnetic field B_y was applied over the scattering chamber and Faraday cup for the parity measurements. The resulting precession of the β -active nuclei about the y direction reduces *those* contributions to R_β which arises from polarization components along z and x . This precaution, which was taken because the results of the activation experiments were not yet available at that time, proved unnecessary in light of the results quoted above. It improves, however, the upper limit for the W beam stop to well below 10^{-9} , since there is no polarization along y .

The final results, $R < 3 \times 10^{-9}$, should be considered a firm upper limit. In particular, the numerical integrations were conservative, especially when combining contributions of opposite sign.

G. Electronic cross talk

A spurious coupling between the signal which determines the polarization state of the ion sources (w or s) and the electronic system used to measure the currents of the Faraday cup and the ionization chamber would produce an additional false asymmetry R_c . To check for such a coupling we made a series of measurements without an accelerator beam, but under test conditions identical to the ones used in the parity runs (e.g., beam profile monitors turning, blower running, ionization chamber with high voltage connected to the integrators). To simulate the beam current, artificial current sources were connected to the Faraday cup and output of the ionization chamber. The result of these tests is given in Table VI.

Test 1 was done with the 14 bit ADC's (note the higher value of the statistical error R_c per minute, mainly due to

TABLE VI. Results of tests for electronic cross talk. The cross talk R_c was measured with the apparatus switched on under realistic conditions, and with the currents from the Faraday cup and ionization chamber simulated by current sources.

Test No.	Time of test	Run time (min)	$\Delta R_c / \text{min}$ (10^{-7})	$R_c \pm \Delta R_c$ (10^{-7})
1	After series 1	6852	12	-0.21 ± 0.16
2	Before series 2	2085	3	-0.15 ± 0.07
3	Before series 2	1806	3	$+0.06 \pm 0.07$
4	After series 2	2546	3	-0.06 ± 0.06

the discretization error), whereas tests 2–4 were made with the 16 bit ADC's. For test 3, the signal which determines whether the weak or strong field transitions are switched on, was reversed. A possible source of electronic coupling which might have led to an asymmetry R_c of about 10^{-8} was found and eliminated after test 3, prior to series 2. However, since electronic cross talk cancels if the measurements with different solenoid field are combined, the systematic error in the final result is well below 10^{-8} and therefore negligible.

H. Periodic modulations

The electronic system is subject to spurious periodic signals, such as pickup of the 50 Hz line frequency, and mechanical noise from the beam scanners through microphonics of the ionization chamber. The tests reported in Table VI show that these signals are averaged sufficiently to present no serious problem. The principal source of periodic modulation not included in the electronic tests is the line-frequency modulation of the proton beam intensity, whose amplitude is a few percent.

The pattern of helicity reversals for the parity measurements was chosen to suppress (i.e., average out) the effects from periodic modulations:

(i) The integration time of 20.0 ms was fixed (quartz clock), and was chosen to correspond to one period of the line frequency of (50.00 ± 0.05) Hz.

(ii) A slow drift in phase between the 20.0 ms integrations and the ac line frequency was introduced by suitable adjustment of the dead time between integrations. The phase drift was $(9 \pm 3)^\circ/\text{s}$.

(iii) The sequence of helicities consisted of groups of 16 measurements:

$$+ - + - + - + - - + - + - + - + - ,$$

or all signs reversed, where the phase reversal in the middle occurs after one revolution of the beam scanners. The starting sign is chosen in a pseudorandom way, such that positive and negative starting sign balance exactly after 128 groups.

We needed to assess whether these measures were sufficient to eliminate errors in R from signals associated with the line frequency or its harmonics. For this purpose, tests were made in which the helicity was alternated in a perfectly regular pattern ($+ - + -$, etc.), phase locked with different phases to the line frequency. Values of $R \approx 10^{-5}$ were observed. This result was confirmed by Fourier analysis of normal parity runs, which revealed no detectable line-frequency component at the level of 10^{-5} . These tests address, besides the effects from line frequency modulation of the beam current, 50 Hz position modulation of the beam, as well as pickup by the electronics (e.g., in the sample-hold circuit). In order to determine by what factor a 50-Hz component in R is reduced by the normal helicity-reversal pattern used, computer simulations were made of 20 min runs with different amounts of phase drift between the 50 Hz signal and the 20.0 ms integrations. The results show that the reduction factor is typically 2×10^{-4} . The remaining effect (2×10^{-9}) is negligible against the statistical error of 5×10^{-7} . Since

the starting phase of the different 20 min runs is random, the effects average out over a large number of runs.

It is also necessary to consider the effects of ac line modulations on the beam scanner data, since the beam is scanned not during but between integrations. Measurements of the corrections R_T and R_M were evaluated for the above-mentioned runs which were phase-locked to the line frequency with different phase ϕ . They show a ϕ dependence of R_T of 15% in amplitude, which again is reduced by a large factor by the normal pattern of helicity reversals. No line frequency component was found in the analysis of runs with the normal helicity pattern. We conclude that line frequency related effects in the beam scanner data are completely negligible.

I. Empty target background and absorption effects

Tests with evacuated target showed that only 97.3% of the current I_s in the ionization chamber is caused by proton scattering in the hydrogen target, the remaining 2.7% being associated with background radiation (neutron, gammas) originating in the beamstop and the windows of the gas target. Thus the measured A_z should be divided by 0.973. A similar small correction in the opposite sense arises from the fact that the measured current I_p in the Faraday cup contains a helicity-dependent contribution of $0.02 \times A_z$ because of the 2% absorption in the gas target. The two effects nearly cancel, and no correction was applied.

The 2.7% background in the ionization chamber may depend on the helicity of the beam if the production of the background radiation involves parity-violating (PV) processes. Since the background arises from many different types of reactions in beamstop and target windows, we assume that the helicity dependence of the background itself, averaged over all background reactions, will at most be a few times 10^{-7} . We therefore assign an uncertainty of 0.2×10^{-7} from this error source to the final result.

V. MEASUREMENTS AND RESULTS

A. Measurements

The measurements were made with the momentum-analyzed beam from the SIN cyclotron. The beam energy incident on the target cell was 50.7 ± 0.1 MeV. The corresponding energy at the effective center of the target (weighted by the acceptance function) is 44.8 MeV, with an rms energy spread of 1.6 MeV.

At the beginning of each running period, the sensitivities to transverse polarizations and to beam position modulation were determined. The nominal position of the beam in the chamber was chosen on the basis of these measurements, as illustrated in Fig. 8 for the coordinates x_1 and x_2 . Since Eq. (4.1) is linear in $\langle x_1 \rangle$ and $\langle x_2 \rangle$, the effect R_T caused by an average transverse beam polarization $\langle p_y \rangle$ vanishes along a straight line which is determined by the three coefficients a_y . The corresponding line is labeled $R_T = 0$ in Fig. 8. Similarly, the effect R_{x_1} (or R_{x_2}) caused by beam position modulation M_{x_1} (or M_{x_2}) vanishes along the straight lines shown in Fig. 8. The

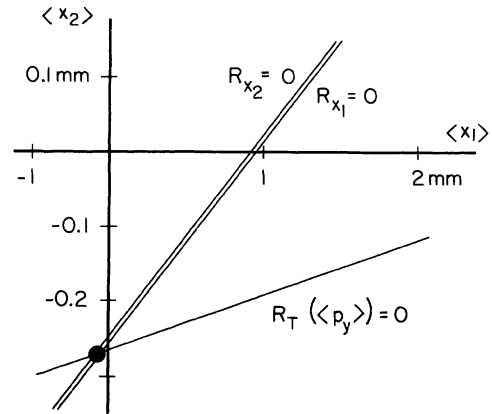


FIG. 8. Choice of the horizontal beam coordinates (solid dot) in the scanners $H1$ and $H2$ for parity measurements. The scale for the $\langle x_2 \rangle$ axis is expanded by a factor of 5. The quantities R are defined in Eqs. (4.1) and (4.6).

nominal beam positions $\langle x_1 \rangle$ and $\langle x_2 \rangle$ for the parity measurements were chosen to minimize these effects. For the example shown, the nominal coordinates (solid dot, Fig. 8) differ from the optical alignment axis (origin of the coordinate system) by 0.3 mm. The coordinates of this nominal beam position was stable to a few tenths of a mm during all experiments, even though the scattering chamber was often disassembled.

During the parity measurements, the beam center normally agreed with the nominal axis within 1 mm in the coordinates x_1 and y_1 and 0.3 mm in x_2 and y_2 . After every six 20-min parity runs, tests were made to measure the sensitivity to position modulations and intensity modulation. In addition, beam breathing and sensitivity to breathing were measured. Beam polarizations p^w and p^s were checked periodically by producing a transversely polarized beam. At the same time the chamber was misaligned to produce a large R_T and thus to check the accuracy of the corrections for transverse polarization $\langle p_y \rangle$.

During each series of parity measurements, the sensitivities to transverse polarization were measured at least twice. In addition, the change in sensitivities with changes in beam current and target pressure were studied. As a matter of principle, the sensitivities were remeasured whenever the apparatus was changed, e.g., for test purposes.

The transverse magnetic field, which was normally applied over the scattering chamber and Faraday cup (Sec. IV F), was reversed every minute in order to maintain, on the average, the axial symmetry of the chamber. Thus all tests and parity measurements were consistently made for an even number of minutes. The proper functioning of all equipment was ascertained by a rigid regime of periodic tests.

B. Evaluations and statistical tests

For each run, the mean value of the asymmetry, R , and the statistical error, ΔR , was calculated in the following way:

(i) The asymmetry $R^{(2)}$ from a pair of 20 ms measurements was calculated according to Eq. (2.1).

(ii) The asymmetry $R^{(16)}$ from a group of 16 measurements (with a random choice of helicity at the beginning, and phase reversal after eight measurements, see Sec. IV H) was calculated as the weighted mean of the eight values $R^{(2)}$.

(iii) The asymmetry R for a 20 min run was calculated as the weighted mean of the $N=20 \times 126=2520$ values $R^{(16)}$. The asymmetry R is assigned a statistical error, ΔR , derived from the variance of $R^{(16)}$:

$$(\Delta R)^2 = \frac{1}{N-1} \sum_{i=1}^N W_i (R_i^{(16)} - R)^2 / \sum_{i=1}^N W_i. \quad (5.1)$$

Here, as well as in (ii) above, the weights W_i are proportional to the charges accumulated in the Faraday cup. Typically, the statistical error of a run with $0.8 \mu\text{A}$ beam current was found to be $\Delta R = 4.5 \times 10^{-7}$. The error expected from the statistical fluctuations in the number of scattered protons is $\Delta R = 3.8 \times 10^{-7}$. The calculation assumed that the charge produced by each proton in the ionization chamber is proportional to the energy loss, where the distribution of energy losses was taken from the calculation described in Sec. III A, while the total number of scattered protons was adjusted to agree with the observed current in the ionization chamber. Statistical fluctuations of charge carriers in the ionization chamber produced by one scattered proton were neglected.

The contribution to ΔR from Poisson statistics of the beam current (shot noise), and from the discretization error of the ADC's, turned out to be small. Shot noise for $I_p = \frac{1}{2} I_s = 0.8 \mu\text{A}$ was calculated to cause an additional error of $\pm 0.19 \times 10^{-7}$ for a 20 min run. The three contributions to ΔR add in quadrature. The observed error ΔR agrees reasonably well with the calculated value. Also, shot noise and discretization error combined explain the statistical error in tests with current sources (Table VI).

Measurements were rejected when the incident beam intensity showed large fluctuations within a group of 16 measurements, specifically when the total charge collected in the Faraday cup for states w and s within a group differed by more than 12%. The average rejection rate was $< 10^{-3}$. The rejections were confined to short periods of unstable cyclotron operation. To guard against gross errors (e.g., transmission errors in the data link) $R^{(16)}$ was tested for deviations from the mean in excess of ten standard deviations, but none were found.

Besides calculating R for each run directly from the $R^{(16)}$ values, we also evaluated the average in several steps in order to judge the statistical consistency. In particular, the χ^2 and corresponding confidence level CL for the average R of each 20 min run was determined in terms of the result for each minute. It was found that out of the total of 69 runs, eleven had a CL below 0.1 and three had a CL below 0.01, which is only slightly worse than expected statistically (seven runs and one run, respectively).

The group asymmetries $R^{(16)}$ were subjected to the following additional tests:

(i) For each run of series 2 (total of 88 000 groups), the mean square successive differences²⁵ of the group asym-

metries were calculated. In the 35 runs we found only one run with significant short period variations, but none with a statistically significant long-term drift.

(ii) The values of $R^{(16)}$ should be distributed according to a normal (Gaussian) distribution with known variance. A χ^2 test of non-normality for the 69 runs showed 11 runs for which the set of 2520 $R^{(16)}$ values was incompatible with a Gaussian distribution of the expected variance (at a confidence level of 1%). Discarding these runs completely, however, changed the final result for A_z only by a small fraction of one standard deviation.

(iii) The asymmetries $R^{(16)}$ from a large sample of runs were ordered according to their magnitude. A so-called robust estimate²⁶ for the center of the distribution is obtained by the "trimmed" mean: of the total of $N=189\,000$ group asymmetries $R^{(16)}$ the $n/2$ highest values and the $n/2$ lowest values are removed and the mean is computed from the remaining $(N-n)$ observations. Even with such a procedure, the final result was very stable. For example, for $n/N=0.3$, we obtained a change of 0.07×10^{-7} in the overall mean value of A_z , well below its statistical error.

The above statistical tests used data which were not corrected for transverse polarization components (correction R_T) or other instrumental effects, since only the integral corrections for entire 20 min runs were available. Experience showed that the corrections R_T often varied significantly from one run to the next, and thus some variation of the corrections *during* a run can be assumed. It is thus plausible that the unsatisfactory χ^2 tests [(ii) above] arise from short-term fluctuations of R_T within the 20 min runs. It must be clearly understood, however, that such fluctuations have no adverse effect on the corrections applied to the results of the 20 min runs, because the parity measurements as well as the beam profiles on which the corrections are based involved the same (beam-intensity weighted) averages over time.

Because tests (i) and (iii) showed no significant irregularities and because the elimination of the "bad" runs from (ii) did not change the final value of A_z in a significant way, all measurements were retained for the evaluation.

C. Results

The systematic uncertainties are collected in Table VII, which lists separately systematic effects which are (a) uncorrelated and (b) correlated for series 1 and 2. Effects are considered uncorrelated if they depend on beam conditions which change from one running period to the next, or if the relevant part of the apparatus was changed between series 1 and 2 so that no correlation is expected.

The final results are summarized in Table VIII. The raw asymmetries R are the error-weighted averages of the uncorrected asymmetries of the 20 min runs, each evaluated as discussed in Sec. V B. The corrected asymmetries, R_z , are the error-weighted averages of the runs corrected individually for transverse polarization components (R_T), intensity modulation (R_0), and, in the case of series 2, beam position modulation (R_M). The error of each run includes, besides the statistical error, Eq. (5.1), a small

TABLE VII. Summary of systematic uncertainties in A_z (in units 10^{-7}).

Systematic uncertainties not correlated for series 1 and 2		
	Series 1	Series 2
Transverse polarization components (R_T , Sec. IV A)	0.2	0.2
Double scattering (R_D , Sec. IV E)	0.5	0.2
Coherent beam modulations:		
Intensity (R_0 , Sec. IV B)	0.2	0.05
Position and angle (R_M , Sec. IV C)	0.1	0.05
Emittance (R_B , Sec. IV C)	0.3	0.05
Energy (R_e , Sec. IV D)	0.2	0.3
Electronic effects (R_c , Sec. IV G)	0.05	0.05
Total systematic uncertainty applied to series 1 and 2 separately	0.69	0.43
Systematic uncertainties correlated for series 1 and 2		
β -decay asymmetry (R_β , Sec. IV F)		0.03
Empty target background (Sec. IV I)		0.2
Beam polarization (Sec. III C)		0.05
Total systematic uncertainty common to series 1 and 2		0.21

TABLE VIII. Summary of results. (The values of R are in units 10^{-7} .)

Series	1		2	
	+	-	+	-
Solenoid				
Number of 20 min runs	24	10	15	20
Raw asymmetry R	-2.65 ± 0.98	1.64 ± 1.50	-8.52 ± 1.15	-2.26 ± 1.04
Corrections:				
Transverse polarization component R_T	1.19 ± 0.09	0.55 ± 0.14	-7.41 ± 0.14	-3.96 ± 0.12
Net correction ($R_T^+ - R_T^-$)		0.32 ± 0.08		-1.73 ± 0.09
Intensity modulation R_0	-1.08 ± 0.01	-1.37 ± 0.02	-1.11 ± 0.01	-0.14 ± 0.01
Net correction ($R_0^+ - R_0^-$)		0.15 ± 0.01		0.01 ± 0.004
Position modulation R_M			-0.20 ± 0.09	-0.01 ± 0.13
Net correction ($R_M^+ - R_M^-$)				0.09 ± 0.08
Corrected asymmetry				
$R_z = \langle R - R_T - R_0 - R_M \rangle$	-2.76 ± 0.99	2.46 ± 1.51	-0.80 ± 1.17	1.85 ± 1.09
$\chi^2/(N-1)$	30.9/23	5.3/9	14.2/14	20.0/19
p_z		0.827		0.830
$A_z = R_z/p_z$	-3.34 ± 1.20	-2.97 ± 1.83	-0.96 ± 1.41	-2.23 ± 1.27
Helicity effect				
$A_z = \frac{1}{2p_z}(R_z^+ - R_z^-)$		-3.16 ± 1.09		-1.60 ± 0.95
Instrumental effect:				
$R_{\text{sol}} = \frac{1}{2}(R_z^+ + R_z^-)$		-0.15 ± 0.90		0.52 ± 0.79
$\chi^2/(N-2)$		36.2/32		34.2/33
rms sum of statistical error and systematic errors in the top part of Table VII		1.30		1.04
Weighted average, series 1 and 2			-2.21 ± 0.81	
Final result (including all systematic errors Table VII)			-2.21 ± 0.84	
$\chi^2/N-1$				72.2/68

contribution from the statistical error of the corrections. For series 1, only an upper limit could be obtained for R_M , because intermittent problems with the data acquisition system prevented reliable corrections for some runs. For this reason, a larger systematic error was assigned to R_M for series 1 (Table VII).

The corrections R_T , R_0 , and R_M , given for positive and negative solenoid excitations separately, are weighted mean values of those corrections which have been applied to each run individually. They demonstrate the effect which corrections have on the raw asymmetries R to obtain the corrected asymmetries R_z . The numbers in the center of each column (net corrections) refer to the correction to R after measurements for opposite solenoid signs are combined. One notes that these corrections are reduced substantially when runs with opposite solenoid sign are combined.

The corrected asymmetries R_z show reasonable χ^2 values. In order to test whether the corrected results contain an unexplained asymmetry which is not proportional to p_z (e.g., from an energy modulation) we calculated an instrumental asymmetry R_{Sol} [Eq. (4.13)]. Its values in Table VIII are consistent with zero. The results for R_{Sol} were used to deduce an upper limit for false asymmetries due to energy modulation (Sec. IV D and Table VII) as a systematic uncertainty.

The final result for the longitudinal analyzing power A_z was obtained in three steps:

(i) Four quantities $A_z = R_z^\pm / p_z$ [Eq. (2.9)] were calculated. The effective beam polarization p_z was obtained by measuring p_y with the precession solenoid turned off. The systematic error which arises from the uncertainty of the $^{12}\text{C}(p,p)^{12}\text{C}$ analyzing power [Eq. (3.1)] is included in Table VII.

(ii) $A_z = \frac{1}{2}(A_z^+ + A_z^-)$ was calculated for series 1 and 2 separately. This average was taken, rather than the error-weighted mean, to cancel possible small undetected effects (e.g., energy modulation) which are independent of p_z . The error of A_z was obtained by adding the systematic errors in the upper part of Table VII quadratically to the statistical error of A_z .

(iii) The final result was obtained as the weighted mean of the two series, and the systematic errors in the lower part of Table VII were added in quadrature.

The final result for the longitudinal analyzing power averaged over the acceptance function of the apparatus is

$$A_z = -(2.21 \pm 0.84) \times 10^{-7}, \quad (5.2)$$

where the error includes statistical and all systematic uncertainties.

The value of $\chi^2/(N-1)$ show for the final result was calculated using the statistical errors only, i.e., with the assumption that after applying the corrections R_T , R_0 , and R_M there are no systematic effects left. The good χ^2 for the 69 runs is obtained only after the corrections listed are applied. Without these corrections, the average has $\chi^2/(N-1) = 141/68$. In Fig. 9 the distribution of A_z for the 69 runs is shown and compared to the expected Gaussian distribution, with excellent agreement.

The list of systematic error sources (Table VII) is complete in the following sense: one can distinguish between

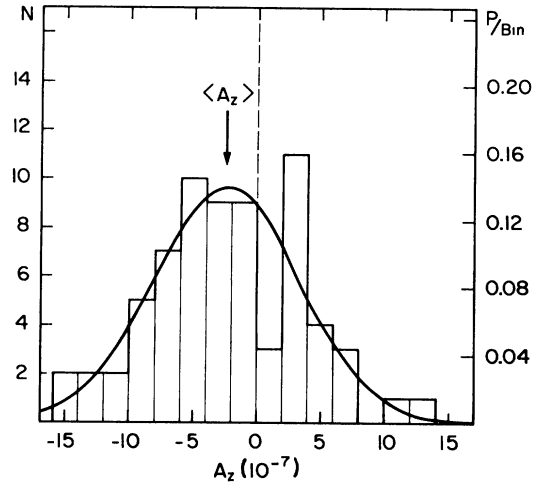


FIG. 9. Statistical distribution of the measured values of the longitudinal analyzing power A_z compared with the theoretical (Gaussian) distribution. The number of runs, N , which yield a value in a given bin is plotted on the left-hand scale, the probability P on the right-hand scale.

effects which are associated with the incident proton beam, and effects which are not. The latter are covered by the electronic tests (Sec. IV G). The former can be divided into two groups: spin effects and phase space effects. The phase space effects are to lowest order covered by the beam modulations listed in Table VII. The spin effects are either from the transverse polarization components (R_T) or due to p_z (R_B , R_D , and PV asymmetry with empty target). Our experience shows that none of the effects discussed can *a priori* be excluded at the accuracy level of 10^{-8} .

The large number of error sources in Table VII should not be taken to indicate that our experiment is subject to more uncertainties than other experiments of this type.^{11,12,14} Rather, it results from a more complete and quantitative treatment than has been presented in other works.

VI. CONCLUSIONS

The quantity usually analyzed theoretically is the longitudinal analyzing power A_z^{tot} of the total nuclear scattering cross sections.^{8,9} Since $A_z(\theta)$ is not entirely independent of angle (see Fig. 3), the value A_z measured for the acceptance functions of our apparatus,

$$A_z = -(2.21 \pm 0.84) \times 10^{-7},$$

differs slightly from A_z^{tot} :

$$A_z^{\text{tot}}(45 \text{ MeV}) = (1.05 \pm 0.05) A_z. \quad (6.1)$$

Thus, the final result of our experiment is

$$A_z^{\text{tot}}(45 \text{ MeV}) = -(2.31 \pm 0.89) \times 10^{-7}. \quad (6.2)$$

Comparison with preliminary results of other experiments at essentially the same proton energy,

$$A_z(46 \text{ MeV}) = -(1.3 \pm 2.3) \times 10^{-7}$$

(Ref. 14) and

$$A_z(47 \text{ MeV}) = -(4 \pm 3) \times 10^{-7}$$

(Ref. 27), shows good agreement. For comparison with the 15 MeV measurements at Los Alamos,^{11,12}

$$A_z^{\text{tot}}(15 \text{ MeV}) = -(1.7 \pm 0.8) \times 10^{-7},$$

one makes use of the fact that

$$A_z^{\text{tot}}(45 \text{ MeV}) = (1.75 \pm 0.1) A_z^{\text{tot}}(15 \text{ MeV}). \quad (6.3)$$

In Eqs. (6.1) and (6.3) the numerical factor is model independent within the error shown (see below). Applying Eq. (6.3) to our result leads to

$$A_z^{\text{tot}}(15 \text{ MeV}) = -(1.3 \pm 0.5) \times 10^{-7},$$

in good agreement with the 15 MeV experiment.

At low energies ($E_p < 100$ MeV), A_z is dominated by the parity nonconserving (PNC) 1S_0 - 3P_0 transition. Thus, $A_z(E_p, \theta)$ can be written as⁸

$$A_z(E_p, \theta) = f(^1S_0\text{-}^3P_0) K_0(E_p, \theta), \quad (6.4)$$

where $f(^1S_0\text{-}^3P_0)$ is the real PNC amplitude defined in Ref. 8, and $K_0(E_p, \theta)$ can be calculated from the known strong p-p phase shifts. The angular dependence K_0 ($E_p = 44.8$ MeV, θ) in Fig. 3, and the numerical coefficients in Eqs. (6.1) and (6.3) were calculated using the p-p phase shifts of Ref. 19. The contribution of the next higher PNC transition, (3P_2 - 1D_2), gives a correction of only a few percent.^{28,29} This correction is model dependent and is responsible for the uncertainties in Eqs. (6.1) and (6.3).

Equation (6.4) allows one to relate A_z^{tot} to $f(^1S_0\text{-}^3P_0)$. We obtain

$$A_z^{\text{tot}}(45 \text{ MeV}) = 2.9 f(^1S_0\text{-}^3P_0), \quad (6.5)$$

which yields

$$f(^1S_0\text{-}^3P_0) = -(0.80 \pm 0.31) \times 10^{-7}. \quad (6.6)$$

Ideally, the experimental results should be compared to calculations based on a fundamental theory of weak interactions such as the standard Glashow-Weinberg-Salam theory. However, strong interactions intervene on several levels in such a program and it is more convenient to proceed in steps. The standard way to analyze parity violating nuclear effects is to relate them to a parity violating nucleon-nucleon interaction based on *one*-boson exchange. The parity violating interaction is thus parametrized by a set of parity violating meson-nucleon coupling constants, which can be determined from experiments and compared to calculations based on a basic weak Hamiltonian in conjunction with quark model and QCD. A comprehensive account of such calculations is given by Desplanques, Donoghue, and Holstein³⁰ (DDH), who arrive for each coupling constant at a rather wide "reasonable range," and a "best guess" value within that range. In p-p scattering, only ρ and ω exchange contribute while one-pion exchange is forbidden by *CP* conservation. Only the following two combinations of the usual isospin (I) labeled coupling constants given in DDH enter therefore:³¹

$$h_\rho^{\text{pp}} = h_\rho^0 + h_\rho^1 + h_\rho^2 / \sqrt{6} = (-15 \pm 20) \times 10^{-7}, \quad (6.7)$$

$$h_\omega^{\text{pp}} = h_\omega^0 + h_\omega^1 = (-3 \pm 8) \times 10^{-7}.$$

The numerical values are the DDH best guess predictions with errors roughly covering the reasonable range.

In order to connect the coupling constants to A_z one has to calculate the PV scattering amplitudes from the one-boson exchange interaction using good nucleon-nucleon wave functions. From the calculations with the Reid soft-core potential³² reported in Refs. 9 and 29 one obtains

$$A_z^{\text{tot}}(45 \text{ MeV}) = 0.74 h_\rho^{\text{pp}} + 0.065 h_\omega^{\text{pp}} \\ = (-1.3 \pm 1.6) \times 10^{-7}, \quad (6.8)$$

where the numerical value is again given by DDH best values with reasonable range. The coefficients in this prediction are roughly doubled³ if one uses super soft core³⁴ wave functions. Although such a procedure is somewhat questionable, since it amounts to regularizing the strong potential but retaining the singularity in the weak one,^{29,3} it nevertheless shows the range of uncertainty due to short range correlations.

Although *one*-pion exchange does not contribute to A_z in the pp system, there is a contribution from 2π exchange. Using the Reid potential and the DDH best value for f_π one obtains at 45 MeV a contribution to A_z of $-0.17 \times f_\pi = -0.78 \times 10^{-7}$ (Refs. 9 and 3). However, in order to contribute, the two pions have to carry the quantum numbers of the ρ meson since their *s*-wave contribution is forbidden by *CP* conservation. It is therefore not clear how much of the 2π contribution should be added explicitly without double counting.

Recently, direct quark model calculations of A_z have been proposed.³⁵ At 100 MeV these calculations predict a very strong angular dependence of A_z , which is hardly physical because they imply large contributions from high partial waves. Clearly more theoretical work is needed for a reliable analysis.

The study of parity violation is now approaching the point where reliable quantitative conclusions are possible, which allow us to test our understanding of the interplay between weak and strong forces in a sector which is not accessible otherwise. Thus we finally ask what further progress can be achieved on the experimental side.

Without doubt, additional experiments of higher precision are needed in order to determine all of the relevant couplings in an unambiguous way. In the pp system, a measurement of A_z in the range of 200–300 MeV could give complementary information to the low energy data, since a different linear combination of h_ρ^{pp} and h_ω^{pp} determines the analyzing power.^{28,29} At these energies, the pp system is still well understood, whereas at higher energies, when inelastic channels are open, the analysis becomes much more difficult.

A direct measurement of A_z in the np system with sufficient accuracy ($< 10^{-7}$) is, unfortunately, very difficult. We, therefore, measured the longitudinal analyzing power in p- α scattering, again at 45 MeV. This target was chosen for its attractive theoretical and experimental

features, i.e., simple nuclear structure and high breakup threshold. The results, which depend in this case sensitively on f_π , will be published elsewhere.

Considerable progress has been made recently in parity violation experiments in ^{18}F , ^{19}F , and ^{21}Ne and their analysis.^{36,37} However, the combination of coupling constants measured in p-p scattering [Eq. (6.8)] is not accessible in these measurements or in p- α scattering. In particular, they are insensitive to h_p^2 .

Since the data presented in this paper were taken, considerable improvements have been achieved in beam condition as well as efficiency of the data acquisition system and other features of our experimental setup. We plan to

resume the p-p experiment in order to achieve an accuracy of a few times 10^{-8} .

ACKNOWLEDGMENTS

Special thanks are extended to the SIN cyclotron operating staff for providing a proton beam which met the special requirements of this experiment, and to Dr. R. Müller for the design of the electronics used in the beam scanner system. We gratefully acknowledge the financial support of the Swiss National Science Foundation. One of us (W.H.) would like to thank the U. S. National Science Foundation for supporting his work.

*Present address: Physik Institut, Universität Basel, CH-4056 Basel, Switzerland.

†Present address: Elektrizitätsgesellschaft Laufenburg, CH-8032, Zürich, Switzerland.

¹W. Haeberli, in *Polarization Phenomena in Nuclear Physics—1980 (Fifth International Symposium, Santa Fe)*, Proceedings of the Fifth International Symposium on Polarization Phenomena in Nuclear Physics, AIP Conf. Proc. No. 69, edited by G. G. Ohlson, R. E. Brown, N. Jarmie, M. W. McNaughton, and G. M. Hale (AIP, New York, 1981), p. 1340.

²B. Desplanques, in *Proceedings of the 8th International Workshop on Weak Interactions and Neutrinos, Javea, Spain*, edited by A. Morales (World Scientific, Singapore, 1983), p. 515.

³M. Simonius, in *High Energy Spin Physics—1982*, Proceedings of the Fifth High Energy Spin Symposium, AIP Conf. Proc. No. 95, edited by Gerry M. Bunce (AIP, New York, 1983), p. 139.

⁴K. S. Krane, C. E. Olsen, and W. A. Steyert, *Phys. Rev. C* **5**, 1663 (1972).

⁵V. M. Lobashov, D. M. Kaminker, G. I. Kharkevich, V. A. Kniazkov, N. A. Lozovoy, V. A. Nazarenko, L. F. Sayenko, L. M. Smoritsky, and A. I. Yegorov, *Nucl. Phys. A* **197**, 241 (1972).

⁶V. A. Knyazkov, E. A. Kolomenskii, V. M. Lobashov, V. A. Nazarenko, A. N. Pirozhov, A. I. Shablii, E. V. Shulgina, Y. V. Sobolev, and A. I. Yegerov, *Nucl. Phys. A* **417**, 209 (1984).

⁷J. F. Caviagnac, B. Vignon, and R. Wilson, *Phys. Lett.* **67B**, 148 (1977).

⁸M. Simonius, *Phys. Lett.* **41B**, 415 (1972).

⁹M. Simonius, *Nucl. Phys. A* **220**, 269 (1974).

¹⁰V. R. Brown, E. M. Henley, and F. R. Krejs, *Phys. Rev. C* **9**, 935 (1974). (The asymmetry A defined in this paper is $2A_z$.)

¹¹J. M. Potter, J. D. Bowman, C. F. Hwang, J. L. McKibben, R. E. Mischke, D. E. Nagle, P. B. Debrunner, H. Frauenfelder, and L. B. Sorenson, *Phys. Rev. Lett.* **33**, 1307 (1974).

¹²D. E. Nagle, J. D. Bowman, C. Hoffmann, J. L. McKibben, R. E. Mischke, J. M. Potter, H. Frauenfelder, and L. B. Sorenson, in *High Energy Physics with Polarized Beams and Polarized Targets (Argonne, 1978)*, Proceedings of the Third International Symposium on High Energy Physics with Polarized Beams and Polarized Targets, AIP Conf. Proc. No. 51, edited by G. H. Thomas (AIP, New York, 1979), p. 218.

¹³R. Balzer, R. Henneck, Ch. Jacquemart, J. Lang, M. Simonius, W. Haeberli, Ch. Weddigen, W. Reichart, and S. Jaccard, *Phys. Rev. Lett.* **44**, 699 (1980).

¹⁴P. von Rossen, U. von Rossen, and H. E. Conzett, in *Polarization Phenomena in Nuclear Physics—1980 (Fifth International Symposium, Santa Fe)*, Proceedings of the Fifth International Symposium on Polarization Phenomena in Nuclear Physics, AIP Conf. Proc. No. 69, edited by G. G. Ohlson, R. E. Brown, N. Jarmie, M. W. McNaughton, and G. M. Hale (AIP, New York, 1981), p. 1442.

¹⁵W. Haeberli, *Annu. Rev. Nucl. Sci.* **17**, 373 (1967).

¹⁶S. Kato *et al.*, *Nucl. Instrum. Methods* **169**, 589 (1980).

¹⁷The material (Perunal 205) for the window foils and the cylinder was supplied by Aluisse, Chippis, Switzerland, and Deutscher Metallhandel, 4300 Essen, Federal Republic of Germany, respectively.

¹⁸H. H. Anderson and J. F. Ziegler, *Hydrogen Stopping Powers and Ranges in All Elements* (Pergamon, New York, 1977), p. 16.

¹⁹R. A. Arndt, L. D. Roper, R. A. Bryon, R. B. Clark, B. J. VerWest, and P. Signell, *Phys. Rev. D* **28**, 97 (1983).

²⁰H. W. Fulbright, *Encyclopedia of Physics* (Springer, Berlin, 1958), Vol. 45, p. 1.

²¹H. F. Glavish, in *Higher Energy Polarized Beams (Ann Arbor, 1977)*, Proceedings of the Workshop on Higher Energy Polarized Proton Beams, AIP Conf. Proc. No. 42, edited by A. D. Kirsch and A. J. Salthouse (AIP, New York, 1978), p. 47.

²²W. Haeberli, R. Henneck, Ch. Jacquemart, J. Lang, R. Muller, M. Simonius, Ch. Weddigen, and W. Reichart, *Nucl. Instrum. Methods* **163**, 403 (1979).

²³M. Simonius, R. Henneck, Ch. Jacquemart, J. Lang, W. Haeberli, and Ch. Weddigen, *Nucl. Instrum. Methods* **177**, 471 (1980).

²⁴Ch. Jacquemart, Ph.D. thesis, Eidgenössische Technische Hochschule, 1981.

²⁵J. von Neumann, R. H. Kent, H. R. Bellison, and B. I. Hart, *Ann. Math. Stat.* **12**, 153 (1941).

²⁶W. T. Eadie, D. Dryard, F. E. James, M. Roos, and B. Sadoulet, *Statistical Methods in Experimental Physics* (North-Holland, Amsterdam, 1971), p. 184.

²⁷D. M. Tanner, Y. Mihara, R. E. Tribble, C. A. Gagliardi, R. E. Neese, and J. P. Sullivan, in *Proceedings of the International Conference on Nuclear Physics, Florence* (Tipografia Compositori, Bologna, 1983), p. F1.

²⁸M. Simonius, in *High Energy Physics with Polarized Beams and Polarized Targets*, edited by C. Joseph and J. Soffer (Birkhäuser, Basel, 1981), p. 355.

²⁹M. Simonius, in *Interaction Studies in Nuclei*, edited by H. Jochim and B. Ziegler (North-Holland, Amsterdam, 1975), p. 3.

- ³⁰B. Desplanques, J. F. Donoghue, and B. R. Holstein, *Ann. Phys. (N.Y.)* **124**, 449 (1980).
- ³¹M. Simonius, *Nucl. Phys.* **A396**, 203c (1983).
- ³²R. V. Reid, *Ann. Phys. (N.Y.)* **50**, 411 (1968).
- ³³The coefficients in Eq. (6.8) are proportional to the strong meson-nucleon coupling constants g_ρ and g_ω which were taken, conventionally, as $g_\rho = g_\omega/3 = 2.7$. The value has been questioned as being too large on the basis of high-energy phenomenology [see G. Nardulli and G. Preparata, *Phys. Lett.* **137B**, 111 (1984)].
- ³⁴R. de Tourel and D. W. L. Sprung, *Nucl. Phys.* **A201**, 193 (1973).
- ³⁵L. S. Kisslinger and G. A. Miller, *Phys. Rev. C* **27**, 1602 (1983).
- ³⁶E. G. Adelberger, M. M. Hindi, C. D. Hoyle, H. E. Swanson, R. D. Von Lintig, and W. C. Haxton, *Phys. Rev. C* **27**, 2833 (1983).
- ³⁷K. Elsener, W. Gruebler, V. König, P. A. Schmelzbach, J. Ulbricht, D. Singg, Ch. Forstner, W. Z. Zhang, and B. Viaridel, *Phys. Rev. Lett.* **52**, 1476 (1984).